Article

Current Biology

A *C9orf72* ALS/FTD Ortholog Acts in Endolysosomal Degradation and Lysosomal Homeostasis

Highlights

- *C. elegans alfa-1* mutations cause yolk release into the extra-embryonic space
- *alfa-1* functions in the degradation of endocytosed material
- Lysosomal reformation and lysosomal homeostasis are altered in *alfa-1* mutants
- *alfa-1* and the human ALS gene *C9orf72* act in similar molecular genetic pathways

Authors

Anna Corrionero, H. Robert Horvitz

Correspondence

horvitz@mit.edu

In Brief

Corrionero and Horvitz show that the *C. elegans* gene *alfa-1* functions in the degradation of endocytosed material and hence has effects on subsequent lysosomal reformation and lysosomal homeostasis maintenance. Human *C9orf72* functions similarly. Aspects of ALS/FTD might result from decreased *C9orf72* function and defective lysosomal degradation.

Corrionero & Horvitz, 2018, Current Biology *28*, 1522–1535
May 21, 2018
https://doi.org/10.1016/j.cub.2018.03.063

CellPress

CellPress

Current Biology
Article

A *C9orf72* ALS/FTD Ortholog Acts in Endolysosomal Degradation and Lysosomal Homeostasis

Anna Corrionero[1] and H. Robert Horvitz[1,2,*]
[1]Howard Hughes Medical Institute, Department of Biology, McGovern Institute for Brain Research, Massachusetts Institute of Technology, Cambridge, MA 02139, USA
[2]Lead Contact
*Correspondence: horvitz@mit.edu
https://doi.org/10.1016/j.cub.2018.03.063

SUMMARY

The most common genetic cause of amyotrophic lateral sclerosis (ALS) and frontotemporal dementia (FTD) is the expansion of a hexanucleotide repeat in a non-coding region of the gene *C9orf72*. We report that loss-of-function mutations in *alfa-1*, the *Caenorhabditis elegans* ortholog of *C9orf72*, cause a novel phenotypic defect: endocytosed yolk is abnormally released into the extra-embryonic space, resulting in refractile "blobs." The *alfa-1* blob phenotype is partially rescued by the expression of the human C9orf72 protein, demonstrating that *C9orf72* and *alfa-1* function similarly. We show that *alfa-1* and *R144.5*, which we identified from a genetic screen for mutants with the blob phenotype and renamed *smcr-8*, act in the degradation of endolysosomal content and subsequent lysosome reformation. The *alfa-1* abnormality in lysosomal reformation results in a general dysregulation in lysosomal homeostasis, leading to defective degradation of phagosomal and autophagosomal contents. We suggest that, like *alfa-1*, *C9orf72* functions in the degradation of endocytosed material and in the maintenance of lysosomal homeostasis. This previously undescribed function of *C9orf72* explains a variety of disparate observations concerning the effects of mutations in *C9orf72* and its homologs, including the abnormal accumulation of lysosomes and defective fusion of lysosomes to phagosomes. We suggest that aspects of the pathogenic and clinical features of ALS/FTD caused by *C9orf72* mutations, such as altered immune responses, aggregation of autophagy targets, and excessive neuronal excitation, result from a reduction in *C9orf72* gene function and consequent abnormalities in lysosomal degradation.

INTRODUCTION

Amyotrophic lateral sclerosis (ALS), a devastating motor neuron disease, shares clinical, neuropathological, and genetic features with frontotemporal dementia (FTD), suggesting that the two diseases might be different manifestations of the same disorder [1, 2]. Supporting this idea, a (GGGGCC) >30 hexanucleotide repeat expansion in a non-coding region of the *C9orf72* gene is the most common genetic cause of both ALS and FTD [3, 4]. Possible pathological mechanisms underlying the neurodegeneration in *C9orf72* ALS/FTD patients include loss of the normal function of C9orf72, expression of repeat-containing RNA, and/or expression of dipeptide-containing proteins generated via unconventional translation [5–13].

Sequence and structural analyses led to the suggestion that *C9orf72* and its homologs in other species are related to differentially expressed in normal and neoplasia (DENN) proteins [14, 15]. DENN proteins act as guanosine diphosphate (GDP)-guanosine triphosphate (GTP) exchange factors for Rab GTPases, small GTPase molecular switches involved in almost all endomembrane-trafficking events in eukaryotes [16]. Recently, C9orf72 has been shown to affect endocytic transport, lysosomal biogenesis, and autophagy, the latter by forming a heterodimer with SMCR8 (Smith-Magenis syndrome chromosome region 8) and regulating Rab39 activity [17–21].

To better understand the normal function of C9orf72, the relationship between C9orf72 function and ALS, and possible toxic effects of drugs designed to decrease hexanucleotide repeat-containing *C9orf72* expression and function, we have analyzed its *Caenorhabditis elegans* ortholog, ALFA-1 (ALS/FTD-associated gene homolog 1) [8, 15] (Figure 1A).

RESULTS

Mutations in the *C. elegans* Ortholog of the ALS Gene *C9orf72* Cause Defects in Yolk Metabolism in the Embryo

Mutations in the *C. elegans* gene *alfa-1*, the ortholog of the human ALS gene *C9orf72*, lead to motor neuron degeneration and stress sensitivity [8]. We discovered a novel abnormal phenotype of embryos with mutations in *alfa-1* (Figure 1A): refractile bodies, which we refer to as "blobs," floating in the extra-embryonic fluid (Figure 1B). These blobs are not membrane bound and do not contain DNA, indicating that they are neither cells nor fragments of cells (data not shown). We generated transgenic animals that expressed fluorescent reporters for the cholesterol-binding yolk proteins VIT-2 [22], VIT-5, and VIT-6 and detected all three reporters in the blobs (Figure 1B; data not shown). *C. elegans* yolk is a lipoprotein complex generated in the intestine of the adult hermaphrodite and transported into the oocyte via receptor-mediated endocytosis. During the morphogenesis stage of embryogenesis when cells

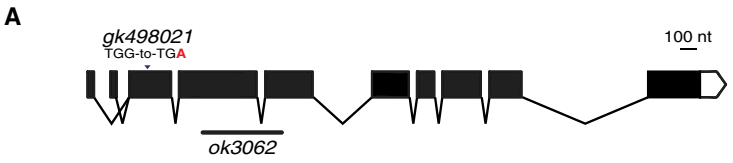

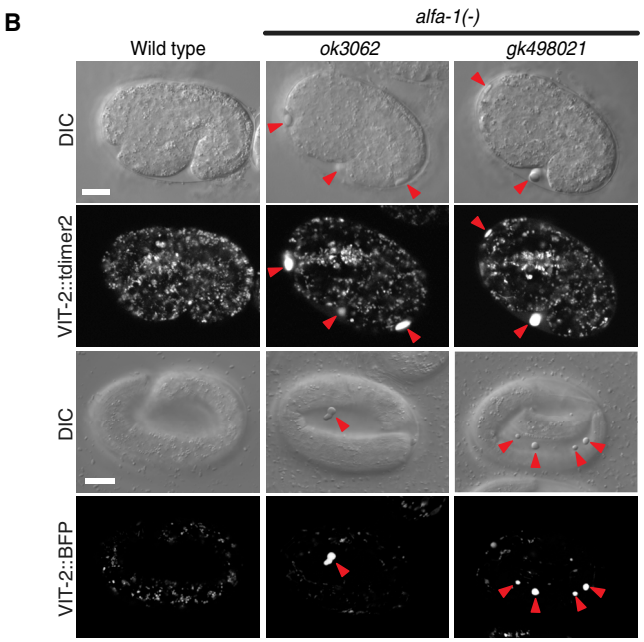

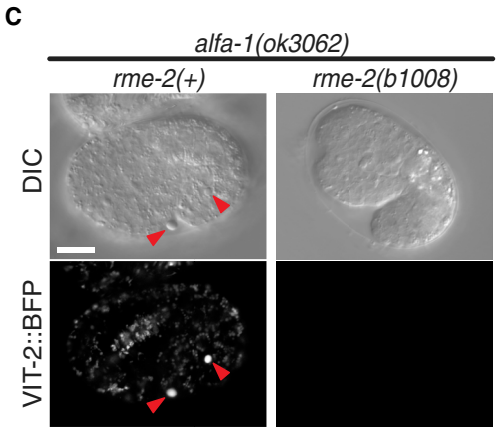

D

Genotype	% animals with blobs (± s.e.m.)
Wild-type	0 ± 0
alfa-1(ok3062)	92.3 ± 1.8
rme-2(b1008)	0 ± 0
alfa-1; rme-2	0 ± 0

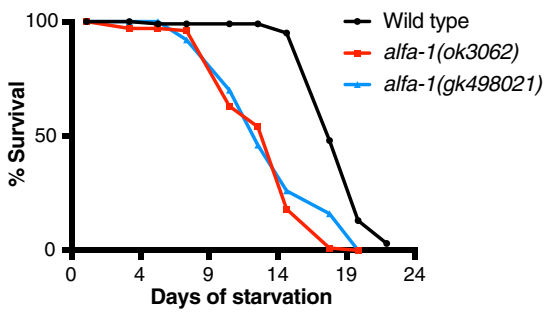

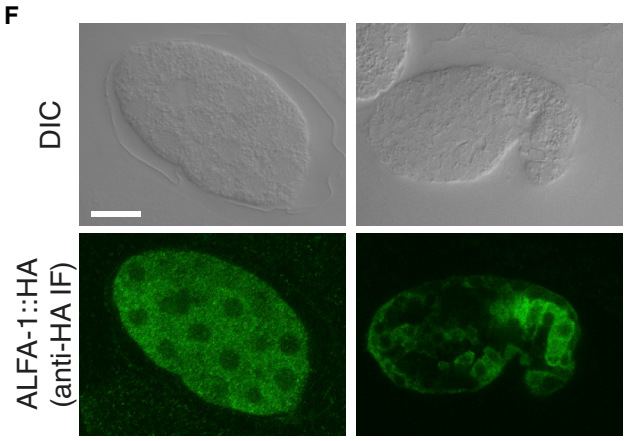

G

Genotype	% animals with blobs (n)
Wild-type	0 (100)
alfa-1(ok3062)	98 (100)
alfa-1; nEx[P$_{alfa-1}$::alfa-1 gDNA] #1‡	6 (100)
alfa-1; nEx[P$_{alfa-1}$::alfa-1 gDNA] #2‡	9 (100)
alfa-1; nEx[P$_{alfa-1}$::ceC9orf72] #1‡	55 (100)
alfa-1; nEx[P$_{alfa-1}$::ceC9orf72] #2‡	59 (100)

Figure 1. *alfa-1* Mutations Cause a Defect in Yolk Storage or Transport in the *C. elegans* Embryo

(A) Genomic organization of *alfa-1*. Two alleles of *alfa-1*, *gk498021* and *ok3062*, are both likely to be null. *gk498021* is a G-to-A transition leading to a tryptophan-to-opal stop codon at amino acid 54, and *ok3062* is a partial deletion of exons 3 and 4. Black bar, sequence deleted in the *ok3062 mutant*.

(B) Differential interference contrast (DIC) and confocal images of wild-type, *alfa-1(ok3062)*, and *alfa-1(gk498021)* comma-stage (top) and 3-fold (bottom) embryos containing the yolk protein transgene *pwIs98[vit-2::tdimer2]* or *nIs755[vit-2::bfp, vit-2::pHluorin]*, respectively. Arrowheads, blobs (abnormal yolk presence in extra-embryonic fluid). Scale bars, 10 μm.

(C) Confocal images of comma-stage embryos of the indicated genotypes containing the transgene *nIs755[vit-2::bfp, vit-2::pHluorin].* Mutation of *rme-2*, the oocyte's yolk receptor gene, suppresses yolk uptake and the blob phenotype. Scale bar, 10 μm. Animals also contained the reporter *qxIs257[nuc-1::mCherry].*

(legend continued on next page)

differentiate, yolk has been reported to be released from non-intestinal cells, transported into the embryonic intestine, and used as an energy source during embryonic development and post-embryonic survival under adverse conditions, such as starvation [23, 24].

Mutations in the oocyte's yolk receptor gene *rme-2* lead to a decreased uptake of yolk by the oocyte [22]. A loss-of-function mutation of *rme-2* suppressed the blob phenotype of *alfa-1(ok3062)* embryos (Figures 1C and 1D), supporting our conclusion that the blobs contain yolk. The *alfa-1* blob phenotype is not caused by an excess uptake of yolk by the oocyte or a defective uptake of yolk by the embryonic intestine, but rather by an abnormal release of yolk from yolk granules into the extra-embryonic fluid at different stages of development (Figures S1A–S1D; data not shown). Released small blobs fuse to generate larger blobs (Figure S1E). Consistent with a defect in yolk [24], *alfa-1* mutants displayed a decreased survival during starvation-induced L1 diapause (Figure 1E). These results suggest that ALFA-1 functions in the storage or degradation of endocytosed yolk in the embryo.

An HA-tagged ALFA-1 translational reporter was expressed ubiquitously during embryonic development and was enriched in the intestine in later stages of embryonic development. ALFA-1 showed a diffuse cytoplasmic localization similar to that of the human C9orf72 long isoform (the isoform more similar to ALFA-1) in HeLa cells and human motor neurons and embryonic kidney cells under basal cell culture conditions (i.e., in the presence of amino acids) [18, 19, 25] (Figure 1F). We determined whether expression of *alfa-1* or a transgene encoding the long isoform of human *C9orf72* and codon-optimized for expression in *C. elegans* (*ceC9orf72*) expressed under the *alfa-1* promoter could rescue the blob phenotype of *alfa-1(ok3062)* embryos. *alfa-1(+)* transgenes almost completely rescued the blob phenotype, while two *ceC9orf72* transgenes partially rescued this defect (Figure 1G), showing that ALFA-1 and C9orf72 most likely function in similar molecular genetic pathways.

We also determined whether we could rescue the blob phenotype by expressing *alfa-1* under different promoters driving its expression in the embryonic intestine, neurons, hypoderm, or ubiquitously. Only the latter led to a complete rescue of the blob phenotype in *alfa-1* embryos, suggesting that *alfa-1* most likely functions cell autonomously in most embryonic cells to regulate yolk homeostasis (Figure S1B; data not shown).

Genetic Interactions between Rab GTPases and *alfa-1* Indicate that ALFA-1 Functions in a Late Step of the Endolysosomal Pathway

To determine at which step in the endolysosomal pathway *alfa-1* functions in yolk storage/degradation, we used RNAi to reduce the functions of putative small Rab GTPases encoded by the *C. elegans* genome [26] and determined how the knockdown of each Rab GTPase affected the penetrance of the blob phenotype in *alfa-1* embryos (Figure 2). We note that when animals were fed the control HT115 bacteria containing the empty vector, the penetrance of the blob phenotype was decreased as compared to OP50-fed animals (Figure S2A), most likely because the progeny of HT115-fed mothers had less yolk than did the progeny of OP50-fed mothers (Figure S2B).

Knockdown of *rab-7* prevented the blob phenotype of *alfa-1* embryos (Figures 2A, 2B, and 2E). Rab7 is found in late endosomes and marks the early-to-late endosome transition [27]. Knockdown of *rab-7* had been previously reported to cause the accumulation of yolk in enlarged endosomes in wild-type embryos [28]. Yolk also accumulated in these abnormal endosomes in *alfa-1* embryos, indicating that *alfa-1* functions after *rab-7* and late endosome formation to promote the appropriate storage and/or degradation of yolk (Figures 2B and 2E, top).

We observed that knockdown of *rab-6.1*, *rab-8*, *rab-11.1*, or *rab-11.2* also suppressed the blob phenotype caused by loss of function of *alfa-1* (Figure 2A). Although we cannot preclude other functions in the storage or degradation of yolk, these Rab GTPases all have been previously implicated in secretion [29–31], suggesting that a decrease in secretion reduces the blob phenotype and consistent with our hypothesis that the blob phenotype is caused by an abnormal release of yolk (Figure 2E, bottom). *rab-10* knockdown also suppressed the blob phenotype; however, animals treated with *rab-10* RNAi and their progeny seemed to have less yolk (data not shown) and most likely reduced the penetrance of the blob phenotype because less yolk was available to be released.

rab-5 and *rab-35* RNAi treatments enhanced the blob phenotype (Figure 2A). RAB-5 regulates early endosome formation after endocytosis, and RAB-35 regulates the endocytic recycling of protein cargo, including of plasma membrane receptors [32, 33]. This result suggests the presence of a reuptake mechanism in which RAB-5 is necessary for the endocytosis of the abnormally released yolk in the embryo while RAB-35 is involved in the recycling of the receptor back to the plasma membrane (Figure 2F, top). Interestingly, loss-of-function mutations in the *ALS2* gene, which encodes a Rab5 activator, cause a recessive, juvenile form of ALS [34, 35]. That a decreased Rab5 function causes ALS is analogous to our finding that decreased *rab-5* function enhances the *alfa-1* blob phenotype. *rab-1* RNAi enhanced the *alfa-1* blob phenotype (Figure 2A). Recently, C9orf72 has been reported to be a Rab1a effector in the regulation of autophagy [20]. Perhaps *rab-1* regulates yolk metabolism partially through the activity of *alfa-1*.

(D) Percentage of 3-fold or older embryos of the indicated genotypes containing blobs, showing the suppression of the *alfa-1* blob phenotype caused by loss of the yolk receptor gene *rme-2* function. For the quantification of the penetrances of the blob phenotype, we studied embryos at the 3-fold stage or older but before the initiation of pumping and derived from 1-day adults, unless otherwise stated. Nomarski differential interference contrast (DIC) optics was used.

(E) Survival curve of wild-type (black), *alfa-1(ok3062)* (red), and *alfa-1(gk498021)* (blue) L1 larvae that hatched in the absence of food. The data shown are representative of two independent experiments.

(F) Anti-HA tag immunofluorescence of proliferative (left) and comma-stage (right) embryos expressing the reporter *nIs759[P_{alfa-1}::alfa-1 gDNA::HA::alfa-1 3′UTR]* showing ALFA-1::HA cytoplasmic localization. Scale bar, 10 μm.

(G) Percentage of 3-fold or older embryos of the indicated genotypes containing blobs. Overexpression of either wild-type *alfa-1* or codon-optimized *C9orf72* for expression in *C. elegans* (*ceC9orf72*) completely or partially rescued the *alfa-1* blob phenotype, respectively. ‡, animals expressed a *P_{alfa-1}::4xnls::gfp::alfa-1 3′UTR* transcriptional reporter. See also Figure S1.

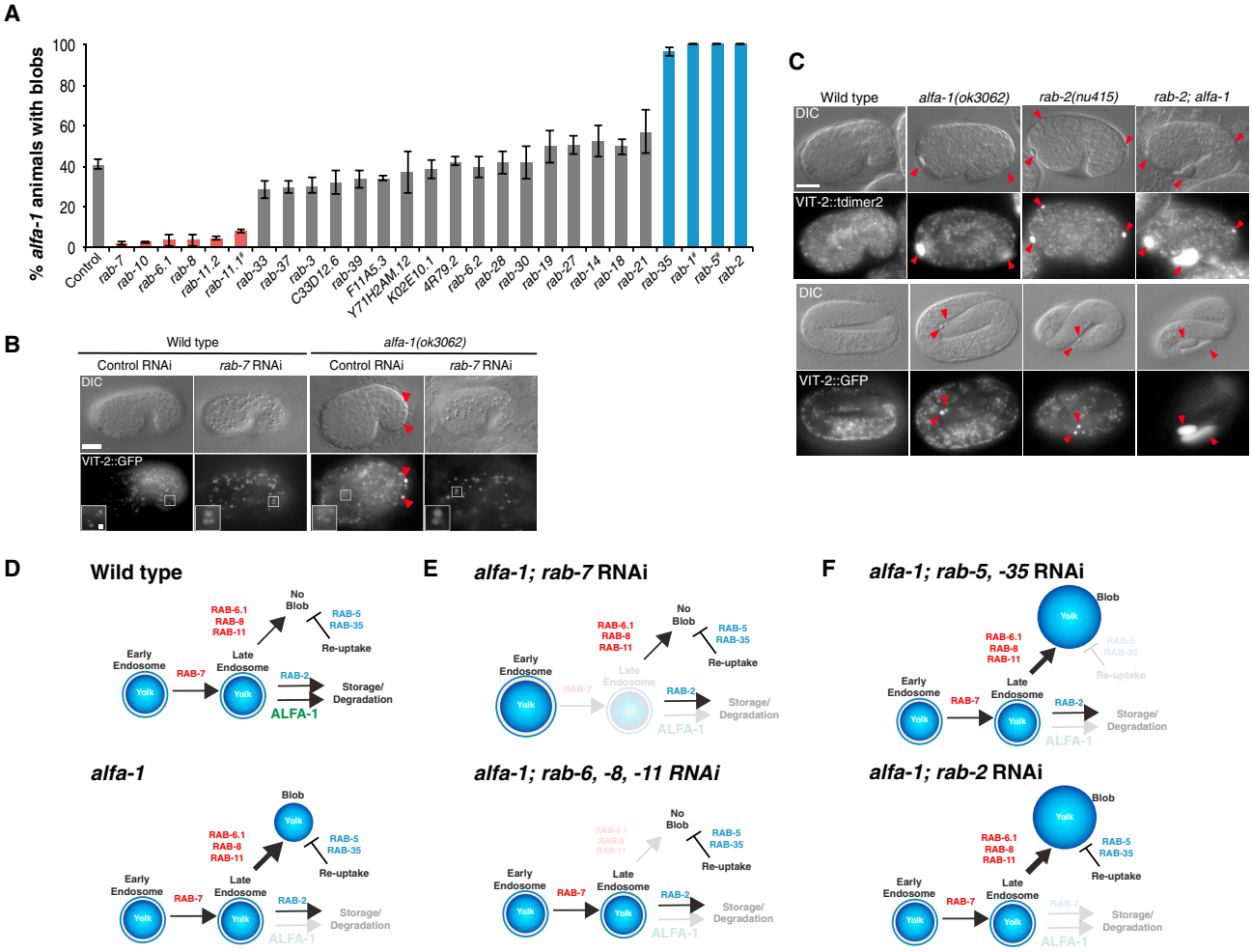

Figure 2. Knockdown of Some Rab GTPases Modulates the *alfa-1* Blob Phenotype and Shows ALFA-1 Acts Late in the Endolysosomal Pathway

(A) *alfa-1(ok3062)* L1 or L4 (#) animals were treated with the indicated RNAi against *C. elegans* Rab GTPase genes [26] and their progeny scored. The average percentage of F1 embryos with blobs from at least three independent experiments is shown. n = 100, except for *rab-1* RNAi where n ≥ 20. Blue bars and red bars correspond to RNAi treatments that enhanced or suppressed the blob phenotype, respectively, in a statistically significant manner (adjusted p value < 0.005, one-way ANOVA test). Error bars, SEM.

(B) DIC and epifluorescene images of comma-stage embryos of the indicated genotypes containing the reporter *pwIs23[vit-2::gfp]* derived from control or *rab-7*-RNAi-treated mothers. *rab-7* knockdown caused the accumulation of yolk in enlarged early and late endosomes in wild-type and *alfa-1* embryos and suppressed the *alfa-1* blob phenotype. Scale bar, 10 μm. Arrowheads, blobs.

(C) DIC and epifluorescence images of comma-stage (top) and late-stage (bottom) embryos of the indicated genotypes containing the reporter *vit-2::tdimer2*. *rab-2* loss of function caused the presence of blobs in the extra-embryonic fluid and enhanced the *alfa-1* blob phenotype, indicating that *alfa-1* and *rab-2* work in different pathways to regulate yolk homeostasis.

(D–F) Proposed genetic pathway that regulates yolk metabolism, showing (D) wild-type and *alfa-1* embryos and the (E) suppression and (F) enhancement of the *alfa-1* blob phenotype after reducing the levels of the indicated Rab GTPases. Light coloring indicates low protein activity. See also Figure S2.

We also observed an enhancement of the blob phenotype upon *rab-2* RNAi treatment. We further analyzed the relationship between the *alfa-1* blob phenotype and *rab-2* using a deletion allele of *rab-2*, *nu415*, a molecular null allele [36]. *rab-2(nu415)* embryos contained blobs, and *rab-2(nu415); alfa-1(ok3062)* double mutants had blobs larger than those of either single mutant (Figure 2C). These data indicate that RAB-2 is also necessary for normal yolk metabolism and that RAB-2 and ALFA-1 most likely work in parallel pathways to regulate yolk storage or degradation (Figure 2F, bottom).

smcr-8, the *C. elegans* Ortholog of the C9orf72-Interacting Protein SMCR8, Functions with ALFA-1 to Regulate Yolk Homeostasis

rab-2 adult hermaphrodites are egg-laying defective and accumulate eggs *in utero* with small blobs. *rab-2; alfa-1* hermaphrodites expressing a *vit-2::gfp* reporter accumulate eggs with large blobs visible as GFP-positive puncta in the mother's uterus (Figure 3A). To identify genes that function in the same pathway as ALFA-1, we performed a genetic screen for enhancers of the *rab-2* blob phenotype (Figure 3A).

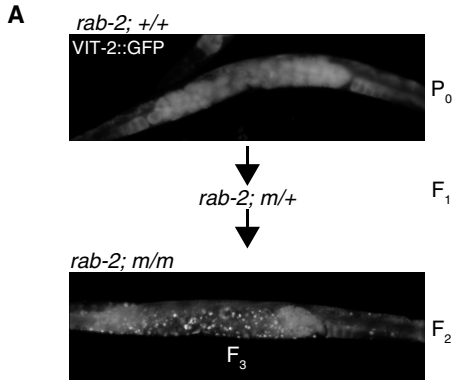

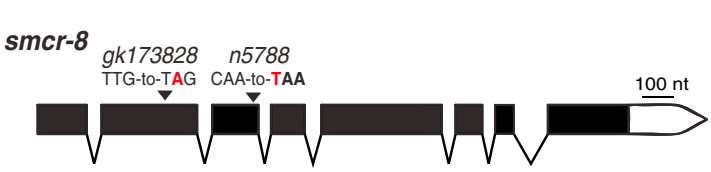

C

Genotype	% animals with blobs (n)
*smcr-8(n5788)**	98 (50)
*smcr-8(n5788); nEx[smcr-8(+)] #1**	4 (50)
*smcr-8(n5788); nEx[smcr-8(+)] #2**	0 (45)
smcr-8(gk173828)	90 (50)
smcr-8(gk173828); nEx[smcr-8(+)] #3	0 (45)
smcr-8(gk173828); nEx[smcr-8(+)] #4	0 (50)

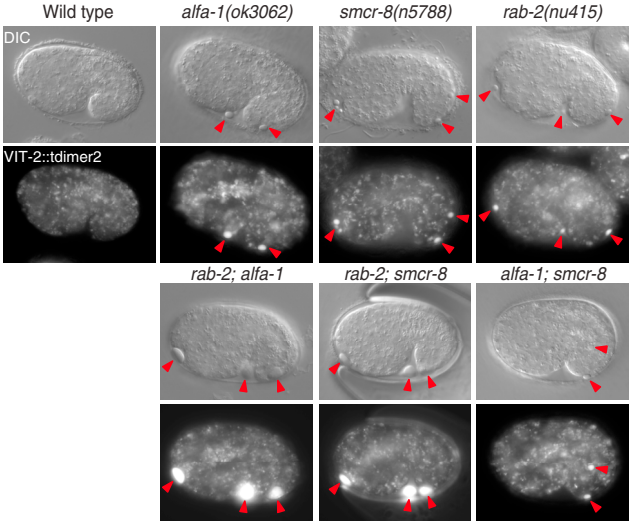

E

Genotype*	% animals with blobs (± s.e.m.)
alfa-1(ok3062)	59 ± 5.4
rab-2(nu415)	67 ± 5.7
smcr-8(n5788)	62 ± 4.0
rab-2; alfa-1	100 ± 0
rab-2; smcr-8	100 ± 0
alfa-1; smcr-8	65 ± 5.0

F

Genotype*	% animals with blobs (± s.e.m.)
smcr-8(n5788); Control RNAi	40 ± 7.3
smcr-8(n5788); rab-7 RNAi	2 ± 0.3

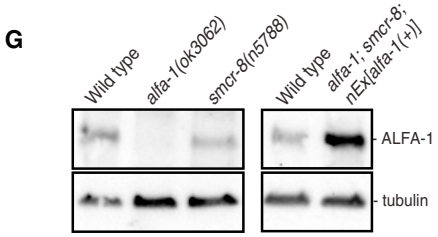

H

Genotype*	% animals with blobs (± s.e.m.)
alfa-1; smcr-8	85.3 ± 2.9
alfa-1; smcr-8; nEx[alfa-1(+)]	82.7 ± 2.4

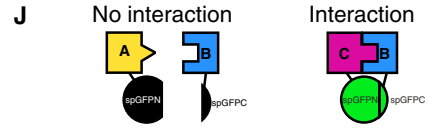

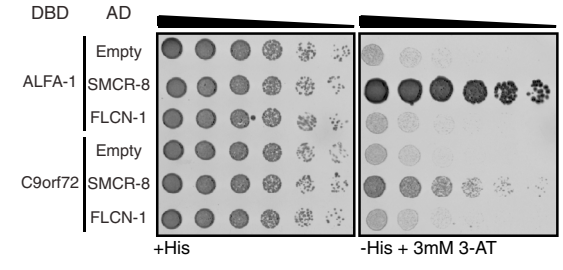

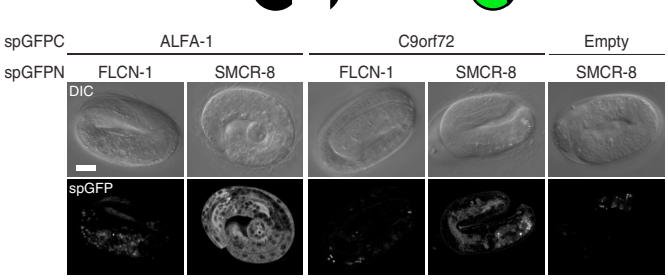

Figure 3. *smcr-8* Functions in the Same Pathway as *alfa-1* to Regulate Yolk Metabolism

(A) *rab-2(nu415)* blob phenotype enhancer screen. Parental generation (P_0) *rab-2* animals were mutagenized, and the F_2 generation was screened for accumulated F_3 eggs with large blobs detected with a *vit-2::gfp* reporter. m, mutation that enhances the *rab-2* blob phenotype.

(legend continued on next page)

The mutation *n5788* both enhanced the *rab-2* blob phenotype and caused blobs by itself (Figures 3C–3E), as do *alfa-1(lf)* mutations. *n5788* is a nonsense mutation in the gene *R144.5* (Figure 3B), the *C. elegans* ortholog of human *SMCR8* (Smith-Magenis syndrome chromosome region, candidate 8). We renamed *R144.5* as *smcr-8*. Another nonsense allele of *smcr-8*, *gk173828* (Figure 3B), phenocopied the *n5788* mutation (Figure 3C). The blob phenotype caused by either *smcr-8* mutation was rescued by overexpressing wild-type *smcr-8* (Figure 3C). These results indicate that *n5788* causes a loss of *smcr-8* function and that *smcr-8*, like *alfa-1*, regulates yolk metabolism and enhances the *rab-2* blob phenotype.

alfa-1; smcr-8 embryos did not have an enhanced blob phenotype compared to that of the single mutants (Figures 3D and 3E), and *rab-7* RNAi also suppressed the *smcr-8* blob phenotype (Figure 3F), indicating that *alfa-1* and *smcr-8* act after late endosome formation in the same pathway to regulate endomembrane-trafficking events.

In HEK cells, C9orf72 levels are greatly reduced upon SMCR8 knockdown [18]. To determine whether ALFA-1 levels are decreased in *smcr-8* mutants, we performed western blot analyses of endogenous ALFA-1 in the wild-type and in *alfa-1* and *smcr-8* mutant embryos. ALFA-1 protein was not detected in *alfa-1(ok3062)* mutants. The levels of ALFA-1 were decreased in the absence of SMCR-8, although apparently to a lesser extent than C9orf72 was decreased in human cell lines. We then asked whether the decreased levels of ALFA-1 could account for the blob phenotype of *smcr-8* mutants. *alfa-1* overexpression did not rescue the blob phenotype of *alfa-1; smcr-8* embryos, indicating that both *smcr-8* and *alfa-1* are necessary for proper yolk homeostasis (Figures 3G, right, and 3H).

Human and mouse SMCR8 can physically interact with C9orf72 to form a complex able to activate Rab39 and Rab8 and promote autophagy [18, 19, 37]. We tested whether *C. elegans* SMCR-8 can physically interact with ALFA-1 and C9orf72 in yeast two-hybrid spot assays. Indeed, SMCR-8 interacted with ALFA-1 and, to a lesser extent, with C9orf72 (Figure 3I). ALFA-1 and C9orf72 did not interact with a control protein, FLCN-1, a DENN-containing protein like both ALFA-1 and SMCR-8, the human ortholog of which, folliculin, is not known to interact with C9orf72 [38]. To validate the physical interaction between ALFA-1 or C9orf72 with SMCR-8 and determine the subcellular localization of this interaction *in vivo*, we used the split GFP (spGFP) system (Figure 3J) [39, 40]. ALFA-1 and C9orf72 were tagged with the C-terminal portion of GFP (spGFPC), while SMCR-8 and FLCN-1 were tagged with an N-terminal fragment of GFP (spGFPN). Only upon physical interaction of proteins containing spGFPC and spGFPN can green fluorescence be detected (Figure 3J). We detected interaction when SMCR-8, but not FLCN-1, was combined with ALFA-1 and, to a lesser extent, with C9orf72 (Figure 3K), validating our yeast two-hybrid spot assay findings. The interactions of ALFA-1 and C9orf72 with SMCR-8 seen in the embryo occurred in the cytoplasm. The decreased interaction between C9orf72 and SMCR-8 compared to that of ALFA-1 with SMCR-8 might explain the partial rescue of the *alfa-1* blob phenotype by the *C9orf72* transgene compared to the *alfa-1* transgene (Figure 1G).

The physical interactions of ALFA-1 and C9orf72 with SMCR-8 indicate that the molecular mechanism of the interaction between *C. elegans* ALFA-1 and SMCR-8 and of that between human C9orf72 and SMCR8 is most likely conserved.

Endolysosome Homeostasis Is Altered in *alfa-1* and *smcr-8* Mutant Embryos

Besides the presence of blobs in *alfa-1* and *smcr-8* mutants, we also noted an abnormal localization of yolk in the heads of mutant embryos. In *alfa-1* and *smcr-8* embryos, yolk granules were localized closer to the lumen of the pharynx than in wild-type embryos (Figures 4A and S3A). This abnormal localization in *alfa-1* and *smcr-8* embryos was rescued by overexpressing wild-type *alfa-1* and *smcr-8*, respectively, confirming that it is the loss of function of these genes that causes this abnormal phenotype (Figure 4A).

(B) Genomic organization of *smcr-8*. The *n5788* nonsense allele isolated from the genetic screen in (A) is a C-to-T transition leading to a glutamine-to-ochre stop codon at amino acid 202. The *gk173828* allele is a T-to-A transversion leading to a leucine-to-amber stop codon at amino acid 122.

(C) Percentage of 3-fold or older embryos of the indicated genotypes containing blobs. *smcr-8* overexpression rescued the blob phenotype of the two different *smcr-8* nonsense alleles. *Animals contained the *vit-2::gfp* reporter.

(D and E) DIC images of embryos containing the (D) *vit-2::tdimer* reporter and (E) average percentage and SEM of the progeny with blobs of embryos of the indicated genotypes from three independent experiments. *smcr-8(n5788)* led to the presence of blobs and enhanced *rab-2(nu415)*, but not *alfa-1(ok3062)*, blob phenotypes, indicating that both *alfa-1* and *smcr-8* work in the same genetic pathway and different from that of *rab-2* to regulate yolk homeostasis. Scale bar, 10 μm. In (E), embryos were derived from HT115-L4440 (control RNAi)-fed mothers to better observe the blob phenotype enhancement (Figure S2). *, animals contained the *vit-2::tdimer2* reporter.

(F) Average percentage of *smcr-8(n5788)* embryos with blobs after treatment with control or *rab-7* RNAi from three independent experiments. SEM is shown. *, animals contained the *vit-2::tdimer2* reporter.

(G) Western blot analysis of ALFA-1 levels in embryos of the indicated genotypes. A western blot using anti-tubulin antibody was the loading control. Animals carried the *vit-2::tdimer2* reporter.

(H) Average percentage of embryos of the indicated genotypes with blobs (three independent experiments). SEM is shown. *Animals carried the *vit-2::tdimer2* reporter.

(I) Yeast two-hybrid spot assay showing the interactions of SMCR-8, but not FLCN-1, with ALFA-1 and C9orf72 in plates without histidine (−His) containing the competitive inhibitor of histidine synthesis 3-AT. Serial one-quarter dilutions were spotted.

(J) Schematic representation of the split GFP (spGFP) method for assessing protein-protein interactions *in vivo*. Animals express a C-terminal GFP fragment (spGFPC) fused to protein B in combination with an N-terminal GFP fragment (spGFPN) fused to proteins A or C. Only physical interaction of the spGFPN- and spGFPC-tagged proteins leads to the emission of green fluorescence.

(K) DIC and confocal images of late-stage embryos expressing an spGFPC fragment fused to ALFA-1, C9orf72, or by itself (empty) in combination with an spGFPN fragment fused to SMCR-8 or FLCN-1. Physical interaction, monitored by the detection of green fluorescence, was detected only when ALFA-1::spGFPC or C9orf72::spGFPC was combined with SMCR-8::spGFPN, but not FLCN-1::spGFPN. Scale bar, 10 μm.

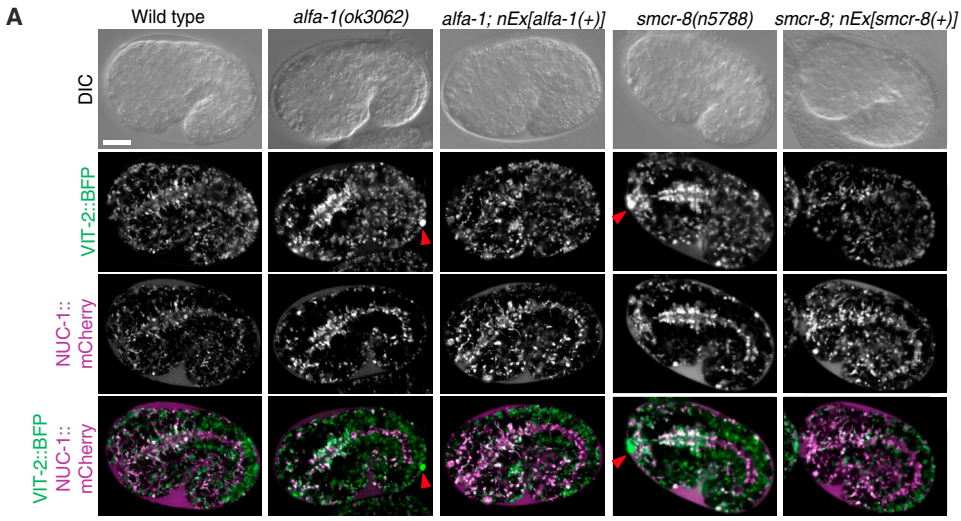

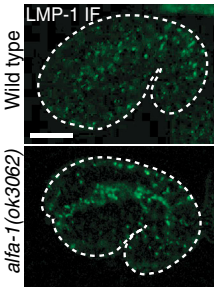

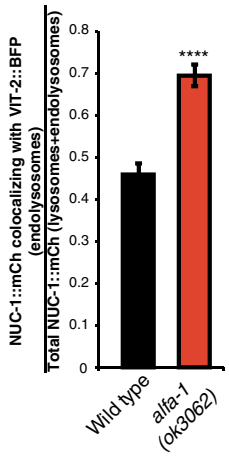

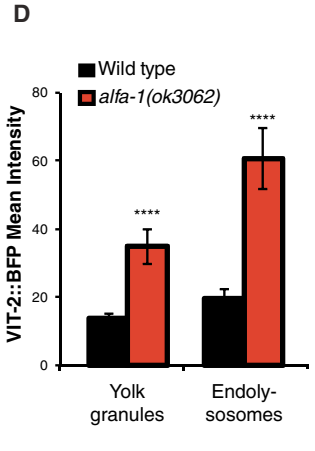

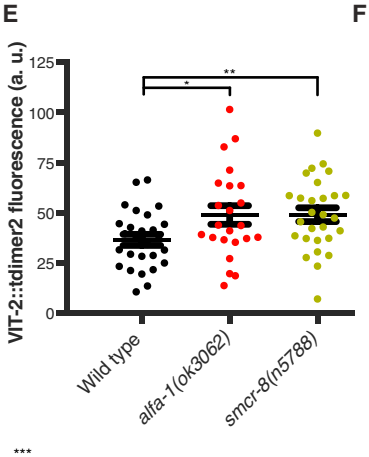

F

Genotype*	% animals with blobs (± s.e.m.)
alfa-1(ok3062)	48.3 ± 8.7
smcr-8(n5788)	41.7 ± 8.2
cup-5(n3264)	2 ± 1.2
glo-1(zu391)	0 ± 0
alfa-1; cup-5	94.0 ± 4.2
alfa-1; glo-1	89.3 ± 4.1
smcr-8 cup-5	87.8 ± 6.5
smcr-8; glo-1	88.1 ± 2.0

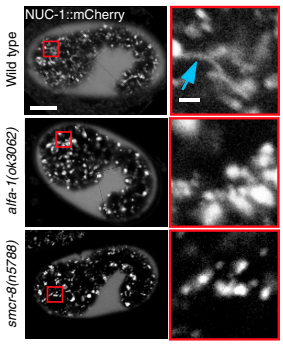

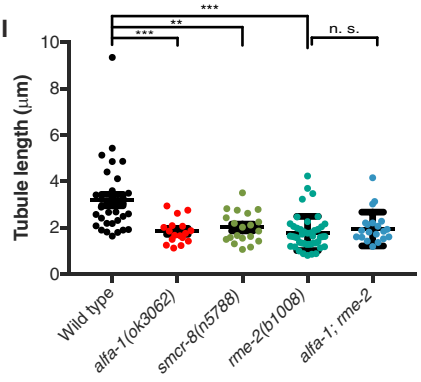

J

Genotype*	% animals with blobs (n)
alfa-1; Control RNAi	48 (50)
alfa-1; rab-7 RNAi	10 (50)
alfa-1; arl-8 RNAi	94 (50)
smcr-8; Control RNAi	58 (100)
smcr-8; rab-7 RNAi	4 (50)
smcr-8; arl-8 RNAi	95 (100)

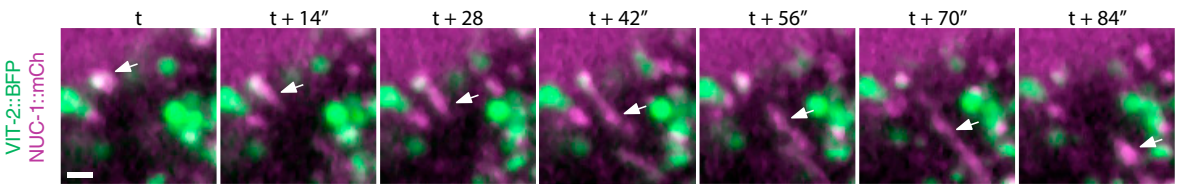

Figure 4. Yolk Degradation Is Abnormal in *alfa-1* and *smcr-8* Mutants

(A) DIC and confocal fluorescence images of embryos of the indicated genotypes containing the reporters *vit-2::bfp* and *nuc-1::mCherry*, showing the abnormal reporter localization in *alfa-1* and *smcr-8* mutants and the rescue of the abnormal localization by *nEx[alfa-1(+)]* or *nEx[smcr-8(+)]* transgenes, respectively. Red arrowheads, blobs. Scale bar, 10 μm.

(legend continued on next page)

We determined whether any of the compartment(s) of the endolysosomal pathway were similarly mislocalized. Endosomes, endoplasmic reticulum (ER), and Golgi all looked grossly normal in *alfa-1* mutant embryos (Figure S3C). However, the lysosomal markers LMP-1 [42] and NUC-1::mCherry [43] showed an abnormal localization similar to that of yolk in *alfa-1* and *smcr-8* mutants (Figures 4A, 4B, and S3B). The abnormal lysosomal localization monitored using the NUC-1::mCherry reporter in *alfa-1* and *smcr-8* embryos was rescued by expressing *alfa-1* or *smcr-8* transgenes, respectively, confirming that *alfa-1* and *smcr-8* are necessary for the normal localization of lysosomes (Figure 4A). We did not observe a decrease in the average intensity of the NUC-1::mCherry reporter in mutant embryos (data not shown), indicating that initial lysosomal biogenesis is not altered in the mutants, in contrast with the recent suggestion of Shi et al. [21] based on their studies of ALS patient induced pluripotent stem cell (iPSC)-derived motor neurons. The abnormal localization of yolk and lysosomal markers is not caused by the presence of blobs, since suppression of the *alfa-1* blob phenotype by *rab-6* RNAi did not alter the abnormal localization of either yolk or the lysosomal marker NUC-1::mCherry (Figure S4).

To further understand the abnormalities of yolk and lysosomal marker localization in *alfa-1* and *smcr-8* mutants, we determined a colocalization coefficient of the lysosomal marker NUC-1::mCherry with the yolk marker VIT-2::BFP (Figure 4C). We defined yolk granules as VIT-2::BFP signal not colocalized with NUC-1::mCherry, lysosomes as NUC-1::mCherry signal not colocalized with VIT-2::BFP, and endolysosomes as the regions where the two fluorescent markers colocalized. The lysosomal marker colocalized significantly more with yolk protein in *alfa-1* mutants than in the wild-type (Figure 4C), indicating that the endolysosomal population was increased in the mutant, possibly because of enhanced endolysosome formation and/or impaired lysosome reformation. We observed that, although wild-type and *alfa-1* oocytes endocytosed similar amounts of yolk (Figures S1A and S2B), the average intensity of VIT-2::BFP in both yolk granules and especially endolysosomes was much higher in *alfa-1* embryos than in wild-type embryos, suggesting that *alfa-1* mutants are defective in yolk degradation (Figure 4D). To verify the abnormal degradation of yolk in the mutants, we quantified the intensity of the VIT-2::tdimer2 reporter in the heads of L1 larvae, where yolk mostly localizes in endolysosomes (data not shown). We note that fluorescently tagged VIT-2 in endolysosomes cannot be detected when using GFP, the fluorescence of which is quenched in the acidic environment of lysosomes. We noticed that *alfa-1* and *smcr-8* L1 animals contained higher levels of the yolk reporter than did wild-type larvae (Figure 4E), consistent with a defect in lysosomal degradation of endocytosed cargo. We also observed defects in the degradation of endocytosed cargo in late larval-stage coelomocytes, macrophage-like cells present in the pseudocoelom (Figure S5A). This finding indicates that defects in the degradation of endocytosed cargo are not limited to the embryo. However, fat degradation was not affected in the intestine of mutant adult animals (Figure S5B).

To further examine the relationship between lysosomal homeostasis and the blob phenotype, we asked whether mutations in *glo-1* or *cup-5* either cause blobs or modify the *alfa-1* or *smcr-8* blob phenotype. *glo-1* is a Rab GTPase involved in the biogenesis of lysosome-related gut granules [44], and *cup-5*, the *C. elegans* ortholog of the human mucolipin 1 gene, is required for normal endolysosomal transport and degradation [45]. We observed that *glo-1(zu391)* mutant embryos did not express the blob phenotype, and only 2% of *cup-5(n3264)* hypomorphic mutant embryos contained blobs (Figure 4F). However, when these mutations were combined with either *alfa-1(ok3062)* or *smcr-8(n5788)*, the blob phenotypes of the *alfa-1* and *smcr-8* mutants were enhanced (Figure 4F). These data support our conclusion that abnormalities in lysosomal homeostasis can lead to the blob phenotype.

We noticed that, in wild-type embryos, lysosomes formed tubular structures, while in *alfa-1* embryos such structures were less obvious and their lengths were decreased (Figures 4G–4I). Lysosomal tubular structures are highly dynamic and in mammals appear after macrophage and dendritic cell activation and during lysosome reformation after lysosomal degradation of vesicular cargo [46]. We performed time-lapse microscopy using the lysosomal reporter NUC-1::mCherry and the yolk protein reporter VIT-2::BFP to determine whether the tubular structures seen in wild-type embryos were indeed lysosomes in the process of being reformed. We observed that lysosomal tubular structures were derived from endolysosomes—as determined by the presence of both yolk and lysosomal markers—contained

(B) Confocal images of the endogenous lysosomal protein LMP-1 in comma-stage embryos showing a distribution similar to that of NUC-1::mCherry. LMP-1 was detected by immunofluorescence (IF) using the anti-LMP-1 antibody described in [41]. Scale bar, 10 μm. Dashed line, embryo outline.

(C) Colocalization coefficients of NUC-1::mCherry with VIT-2::BFP (i.e., ratio of NUC-1::mCherry-positive pixels colocalizing with VIT-2::BFP in endolysosomes to sum of total NUC-1::mCherry-positive pixels) in comma-stage embryos of the indicated genotypes. $n \geq 10$. Error bars, SEM. ****$p < 0.0001$ (Student's t test).

(D) Quantification of VIT-2::BFP mean fluorescence intensity in comma-stage embryos of the indicated genotypes in yolk granules or endolysosomes. $n = 11$. Error bars, SEM. ****$p < 0.0001$ (Student's t test).

(E) Average intensity of VIT-2::tdimer2 fluorescence in the heads of L1 larvae of the indicated genotypes. Error bars, SEM. *$p < 0.05$ and **$p < 0.01$ (Student's t test).

(F) Average percentage of embryos of the indicated genotypes with blobs (three independent experiments). Embryos were derived from HT115-L4440-fed mothers. *Animals contained the *nuc-1::mCherry* and the *vit-2::BFP; vit-2::pHluorin* reporters.

(G) 1.5-fold embryos of the indicated genotypes carrying the reporter NUC-1::mCherry detected in hypodermal cells. In wild-type embryos, the lysosomal marker accumulates in small aggregates and tubular structures (blue arrow), while in *alfa-1* and *smcr-8* mutants the lysosomal marker accumulates mostly in larger aggregates. Scale bar, 10 μm. Red box, inset. Inset scale bar, 1 μm.

(H) Time-lapse confocal microscopy starting at time t, showing the formation of a lysosomal tubular structure from an endolysosome and subsequent lysosomal reformation in a wild-type embryo carrying the lysosomal marker NUC-1::mCherry (purple) and the yolk marker VIT-2::BFP (green). Maximum-intensity projection along the z axis of three slices is shown. Arrows indicate reformation tubules. Scale bar, 1 μm.

(I) Average length of lysosomal tubules in embryos of the indicated genotypes. Error bars, SEM. **$p < 0.01$ and ***$p < 0.001$ (Student's t test). $n \geq 5$ embryos.

(J) Percentage of F1 *alfa-1* and *smcr-8* embryos with blobs derived from P_0 worms treated with the indicated RNAi clones. See also Figures S3–S5.

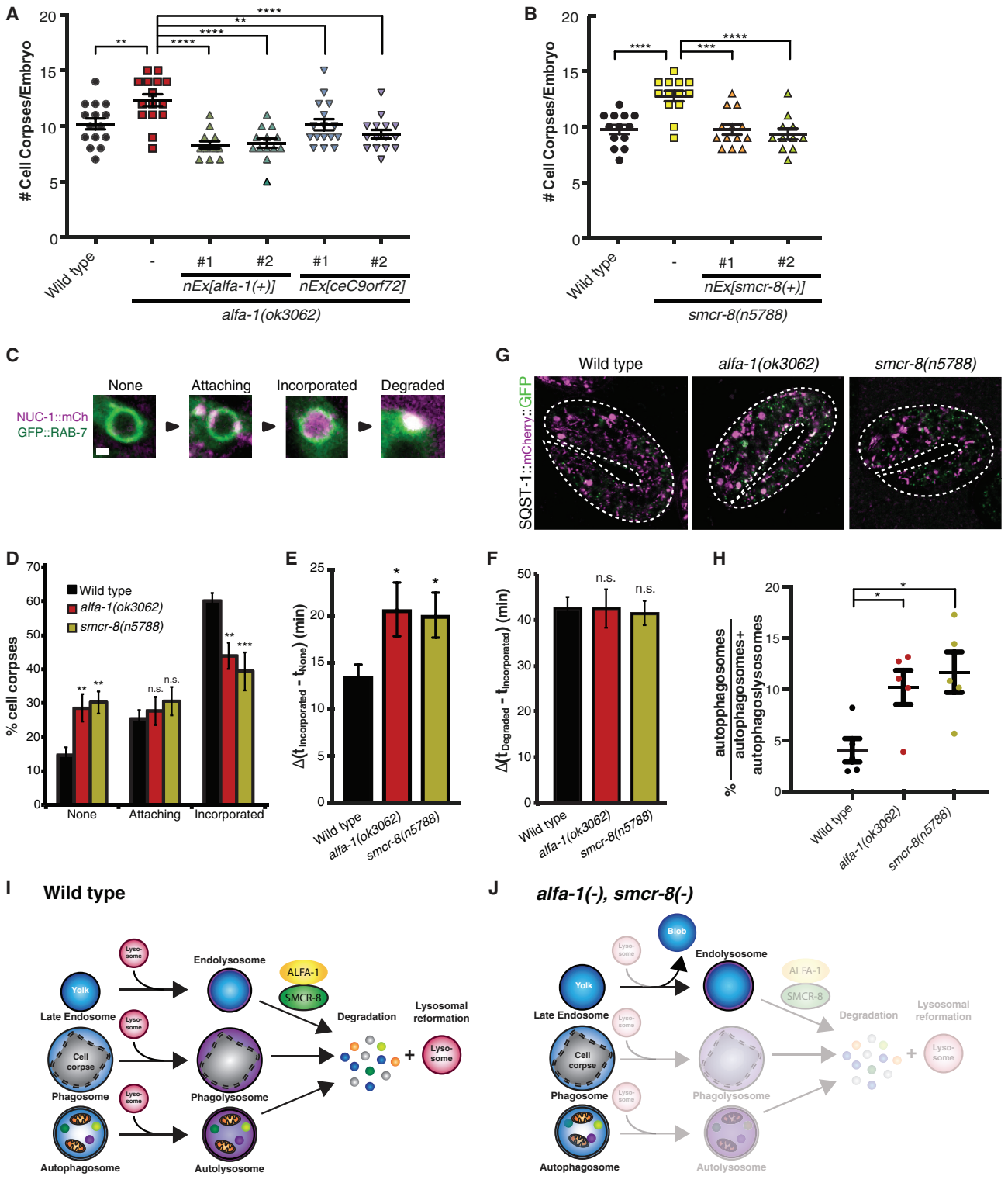

Figure 5. Defective Lysosomal Degradation Leads to the Accumulation of Cell Corpses and Substrates for Autophagy

(A and B) Average number of cell corpses scored in the heads of (A) *alfa-1* or (B) *smcr-8* 1.5-fold embryos. *nEx[alfa-1(+)]*, *nEx[ceC9orf72]*, and *nEx[smcr-8(+)]* indicate overexpression of *alfa-1*, *ceC9orf72*, or *smcr-8* rescuing constructs, respectively. n ≥ 13 embryos. Error bars, SEM. One-way ANOVA with Bonferroni post hoc test and Student's t test for (A) and (B), repectively; $^{**}p < 0.01$ and $^{****}p < 0.0001$.

(legend continued on next page)

little or no VIT-2::BFP reporter, and after formation underwent scission to reform lysosomes (Figure 4H). Tubules in *alfa-1* and *smcr-8* mutants were shorter (Figure 4I) and less abundant (*alfa-1* = 2.1 ± 0.5, *smcr-8* = 2.9 ± 0.6, and wild-type = 5.8 ± 0.7 tubules/embryo ± SEM) than those in wild-type embryos. A decrease of yolk content in the embryo caused by a mutation in the yolk receptor *rme-2* led to a decrease in tubule length in *rme-2*, but not in *alfa-1; rme-2* mutants, as compared to wild-type and *alfa-1* embryos, respectively (Figure 4I), and to a suppression of the number of tubules per embryo caused by the loss of *alfa-1* (*rme-2* = 7.5 ± 0.8, *alfa-1; rme-2* = 5.3 ± 0.3 tubules/embryo ± SEM; $p > 0.5$). Although this effect of low levels of embryonic yolk on lysosomal tubule length remains to be understood, the suppression of the defect in the number of tubules per embryo caused by *alfa-1* loss of function in the *alfa-1; rme-2* double mutant is consistent with a dependence of lysosomal reformation on there being a low amount of yolk in endolysosomes.

We asked whether knockdown of the Arf-like small GTPase *arl-8* would modify the *alfa-1* and *smcr-8* blob phenotypes, since mammalian Arl8 is necessary for lysosomal tubulation in macrophages [47]. Decreased *arl-8* levels led to an enhanced blob phenotype (Figure 4J). We suggest that *arl-8* RNAi treatment enhanced the defect in lysosomal reformation seen in *alfa-1* and *smcr-8* mutants, reducing the number of lysosomes available to degrade yolk and leading to an enhanced abnormal release of yolk in *alfa-1* and *smcr-8* mutants.

In short, our data indicate that the defect in yolk degradation is likely to be responsible for the observed defects in lysosomal reformation in *alfa-1* embryos, since lysosomal degradative function is required for lysosomal reformation [46] and the blob phenotype. However, it remains possible that an increase in degradation of lysosomes is a contributing factor to the decreased lysosomal population compared to the endolysosomal population in the *alfa-1* mutant embryos.

Mutations in the gene that encodes the lysosomal membrane protein *scav-3* decrease the formation of tubular lysosomal structures [48]. However, we did not detect the presence of blobs, the abnormal localization of endolysosomes in the pharynx, or a defect in the degradation of yolk in *scav-3(tm3659)* deletion mutant embryos, suggesting that the mechanism by which *scav-3* mutations lead to defective lysosomal tubulation is different from that of *alfa-1* and *smcr-8* mutations.

Defective Lysosomal Homeostasis Leads to the Accumulation of Cell Corpses and Substrates for Autophagy

Lysosomes can fuse with late endosomes, phagosomes, and autophagosomes to promote the degradation of their cargoes. Phagocytosis and autophagy are essential processes that degrade large foreign particles and cytoplasmic constituents, respectively. We asked whether the lysosomal degradation of cargo derived from phagocytosis (apoptotic cell corpses) and autophagy (SQST-1) was defective in *alfa-1* and *smcr-8* embryos.

We determined the number of cell corpses in the heads of 1.5-fold-stage embryos. Compared to wild-type embryos, *alfa-1* and *smcr-8* mutants showed an excess of cell corpses (Figures 5A and 5B). Overexpression of either *alfa-1(+)* or *ceC9orf72* transgenes completely or partially rescued, respectively, the corpse defect of *alfa-1* mutants (Figure 5A), and overexpression of *smcr-8(+)* rescued the *smcr-8* cell corpse defect (Figure 5B).

Excess cell corpses might be caused by either excessive cell death or a defect in the engulfment or degradation of engulfed cell corpses. To assess the latter, we determined the recruitment of lysosomes to vesicles containing phagocytosed cell corpses [43]. RAB-7-positive cell corpse-containing phagosomes fuse with lysosomes to form phagolysosomes and degrade their content (Figure 5C). *alfa-1* and *smcr-8* embryos showed a decrease in phagolysosome formation (incorporated lysosomes) and an increase in the percentage of phagosomes with no lysosomes attached (Figure 5D). This defect is consistent with the longer time needed for the incorporation of lysosomes in RAB-7-positive cell corpse-containing phagosomes after RAB-7 clustering around phagosomes in the mutant embryos (Figure 5E), while the average time period for the degradation of cell corpses after incorporation of lysosomes was similar between wild-type and *alfa-1* and *smcr-8* mutant embryos (Figure 5F). These results suggest that the defective degradation of yolk and decreased lysosomal reformation lead to a decrease in available lysosomes to be recruited to apoptotic cell-containing phagosomes, causing a defect in apoptotic cell clearance.

We asked whether autophagic flux also is impaired in *alfa-1* and *smcr-8* embryos. SQST-1, the *C. elegans* homolog of SQSTM1/p62 (sequestosome 1), is selectively removed by autophagy during embryogenesis [50]. To monitor the autophagic flux in wild-type and mutant embryos, we generated an SQST-1::mCherry::GFP dual fluorescent reporter. This reporter

(C) Time-lapse images of RAB-7::GFP-positive, cell corpse-containing phagosomes with no lysosomes (None), with attaching lysosomes (attaching), and with incorporated lysosomes (Incorporated) that will result in the degradation of the cell corpse (degraded). Scale bar, 1 μm.

(D) Percentage of cell corpse-containing phagosomes displaying different NUC-1::mCherry localization as classified in (C) for the genotypes indicated. $n \geq 90$ corpses, and at least seven 1.5-fold embryos. Error bars, SEM. n.s., $p > 0.05$; $^{**}p < 0.01$ and $^{***}p < 0.001$.

(E) Average time from the formation of a RAB-7-positive cell corpse-containing phagosome (t_{none}) until the incorporation of lysosomes ($t_{incorporated}$) leading to the formation of phagolysosomes. $n \geq 13$ cell corpses. Error bars, SEM. $^{*}p < 0.05$ (Student's t test).

(F) Average time from the incorporation of lysosomes ($t_{incorporated}$) until the complete degradation ($t_{degraded}$) of the C1, C2, and C3 cell corpses [49]. $n \geq 5$ cell corpses. Error bars, SEM. n.s., $p > 0.05$.

(G) Confocal fluorescence images of 2-fold embryos of the genotypes indicated containing the reporter *nIs845[sqst-1::mCherry::gfp]*, showing defective fusion of lysosomes with autophagosomes in *alfa-1* and *smcr-8* embryos.

(H) Average percentage of autophagosomes (GFP- and mCherry-positive particles) of all SQST-1-containing particles (i.e., autophagosomes and autophagolysosomes). n = 5 embryos. Error bars, SEM. $^{*}p < 0.05$ (one-way ANOVA).

(I) In wild-type animals, lysosomes fuse with endosomes, phagosomes, and autophagosomes to generate endolysosomes, phagolysosomes, and autolysosomes, respectively, leading to the degradation of their contents. After degradation, lysosomes are reformed.

(J) In *alfa-1* or *smcr-8* embryos, lysosomes fuse with endosomes, but both degradation of yolk and lysosome reformation are impaired, leading to the abnormal release of yolk to the extra-embryonic fluid. Defects in the formation of phagolysosomes and degradation of autophagosomal content are also observed.

exploits the different sensitivities of GFP and mCherry fluorescence to quenching in low-pH environments: the GFP signal, but not the mCherry signal, is quenched by the acidic pH in autophagolysosomes [51]. Hence, this reporter labels autophagosomes and autophagolysosomes as GFP-positive and mCherry-positive particles or as only mCherry-positive particles, respectively. We observed that, in both *alfa-1* and *smcr-8* embryos, the percentage of autophagosomes was higher than in wild-type embryos, indicating a defect in autophagolysosome formation in the mutants (Figures 5G and 5H). Mutations in the *C. elegans* orthologs of the autophagy genes *ULK1* and *p62/sequestosome*, *unc-51(e1189)* and *sqst-1(ok2892)*, respectively, did not cause the blob phenotype, and knockdown of *let-363*, the *C. elegans* ortholog of the autophagy inhibitor mTOR, did not affect the *alfa-1*, *smcr-8*, or *rab-2* blob phenotypes (data not shown), indicating that it is not the impaired autophagy in *alfa-1* and *smcr-8* mutants that leads to the blob phenotype. Using an SQST-1::GFP reporter, we detected an accumulation of the reporter in the heads of *alfa-1* and *smcr-8* adults (Figure S5C), indicating altered autophagy in the mutants. This defective autophagy is consistent with the hypothesis that loss of *C9orf72* function contributes to neurodegeneration—which might be caused by the accumulation of misfolded and aggregated proteins in C9orf72 ALS patients—as previously proposed based on studies of mouse and human cell lines [19, 37, 52].

Our data indicate that *alfa-1* and *smcr-8* are necessary for the maintenance of lysosomal homeostasis and that mutations in either of these genes lead to defective lysosomal degradation of endosomal, phagosomal, and autophagosomal cargo.

DISCUSSION

Mutations in *alfa-1*, the *C. elegans* ortholog of the ALS/FTD gene *C9orf72*, lead to motor neuron degeneration and stress sensitivity [8]. Here we describe a novel phenotype of *alfa-1* mutants—the abnormal release of yolk into the extra-embryonic fluid. From our analysis of *alfa-1*, we discovered the function of a *C9orf72* homolog: *alfa-1* acts in the degradation of endocytosed material, in lysosomal reformation, and in the general maintenance of lysosomal homeostasis (Figures 5I and 5J).

Our data indicate that *C. elegans alfa-1* and human *C9orf72* function in similar genetic molecular pathways, since (1) expression of the long isoform of human *C9orf72* can partially rescue the *alfa-1* mutant phenotype, and (2) from a genetic screen for additional mutations that cause the blob phenotype, we identified *R144.5*, the *C. elegans* ortholog of *SMCR8*, a protein that has been reported recently to interact physically with C9orf72 to regulate autophagy [19, 37, 52].

Our findings about the function of *alfa-1* in the degradation of endocytosed material and the maintenance of lysosomal homeostasis explain apparently disparate previous observations concerning effects of the loss of *C9orf72* function, such as (1) the abnormal accumulation of lysosomes and aggregates of the autophagy target p62/sequestosome seen in *C9orf72* knockout mice, human cells depleted of *C9orf72*, and *C9orf72* ALS/FTD patients [20, 37, 53–55]; and (2) the defective fusion of phagosomes to lysosomes seen in *C9orf72*-knockout mice [53].

The dominant inheritance of the ALS/FTD caused by a hexanucleotide repeat expansion in *C9orf72* and the lack of *C9orf72*-coding mutations in ALS/FTD patients suggest a gain-of-function pathogenic mechanism for the repeat expansion [3, 4]. Nonetheless, some clinical features of ALS/FTD might result from a reduction or loss of C9orf72 function. For example, a recent study showed that haploinsufficiency of *C9orf72* leads to neurodegeneration of ALS patient iPSC-derived motor neurons in the presence of elevated glutamate levels or upon expression of the Proline-Arginine dipeptide-containing protein associated with C9orf72 ALS [21]. Based on our observations of *alfa-1* mutants, we suggest that *C9orf72* decreased function would similarly cause defects in lysosomal degradation and an abnormal release of vesicular contents, and in that way contribute to the systemic inflammatory response seen in ALS patients [56] and/or to the excessive glutamate release leading to neuronal excitotoxicity caused by overactivation of excitatory glutamate receptors, a process that has been suggested to be a pathogenic mechanism in ALS [57]. In addition, decreased function of *C9orf72* might result in the abnormal degradation and consequent release of pathogenic dipeptide-repeat proteins—the products of the translation of repeat expansion-containing RNAs—promoting their cell-to-cell prion-like spreading and non-autonomous cell toxicity [58] and, thereby, augmenting the *C9orf72*-driven disease process. Also, the consequences of the loss of *alfa-1* function suggest potential toxic effects of drugs that target *C9orf72* with the goal of ameliorating RNA and/or dipeptide repeat-containing protein pathogenicity.

STAR★METHODS

Detailed methods are provided in the online version of this paper and include the following:

- KEY RESOURCES TABLE
- CONTACT FOR REAGENT AND RESOURCE SHARING
- EXPERIMENTAL MODEL AND SUBJECT DETAILS
- METHOD DETAILS
  - Plasmids
  - Germline transformation
  - Starvation survival assay
  - Microscopy, immunohistochemistry and image analysis
  - Counts of blobs and persistent corpses
  - Genetic screen and mapping of smcr-8(n5788)
  - Antibody production and western blot analysis
  - Yeast two-hybrid binding assay
  - Oil Red O (ORO) staining and imaging
  - ceC9orf72 sequence
- QUANTIFICATION AND STATISTICAL ANALYSIS

SUPPLEMENTAL INFORMATION

Supplemental Information includes five figures and two tables and can be found with this article online at https://doi.org/10.1016/j.cub.2018.03.063.

ACKNOWLEDGMENTS

We thank P. Agbu, Z. Zhou, B. Grant, A. Kimura, X. Wang, G. Ou, D. Lee, S.V. Lee, and M.E. Gallegos for providing strains and constructs; R. Droste for determining DNA sequences and RNAi library management; N. An and T. Ljungars for strain management; N. Bhatla, K. Burkhart, D. Denning, A. Doi, T.

Hirose, S. Luo, and N. Paquin and other members of the Horvitz laboratory for discussions; R.H. Brown, J. Valcárcel, and Z. Zhou for suggestions concerning the manuscript; and the *Caenorhabditis* Genetic Center, which is funded by the NIH Office of Research Infrastructure Programs (P40 OD010440), and the National BioResource project for strains. A.C. was supported by an EMBO postdoctoral long-term fellowship (ALTF 144-2011). An ALS Therapy Alliance grant (2013-S-0113) and gifts from Mr. and Mrs. D.C. Barnard to the MIT McGovern Institute and the Halis Family Foundation to the MIT Aging Brain Initiative helped support this research. H.R.H. is the David H. Koch Professor of Biology at MIT and an Investigator at the Howard Hughes Medical Institute.

AUTHOR CONTRIBUTIONS

Conceptualization, A.C. and H.R.H.; Methodology, A.C.; Investigation, A.C.; Writing – Original Draft, A.C. and H.R.H.; Funding Acquisition, A.C. and H.R.H.; Resources, A.C. and H.R.H.; Supervision, H.R.H.

DECLARATION OF INTERESTS

The authors declare no competing interests.

Received: July 21, 2017
Revised: February 18, 2018
Accepted: March 27, 2018
Published: May 3, 2018

REFERENCES

1. Lillo, P., and Hodges, J.R. (2009). Frontotemporal dementia and motor neurone disease: overlapping clinic-pathological disorders. J. Clin. Neurosci. *16*, 1131–1135.
2. Neumann, M., Sampathu, D.M., Kwong, L.K., Truax, A.C., Micsenyi, M.C., Chou, T.T., Bruce, J., Schuck, T., Grossman, M., Clark, C.M., et al. (2006). Ubiquitinated TDP-43 in frontotemporal lobar degeneration and amyotrophic lateral sclerosis. Science *314*, 130–133.
3. DeJesus-Hernandez, M., Mackenzie, I.R., Boeve, B.F., Boxer, A.L., Baker, M., Rutherford, N.J., Nicholson, A.M., Finch, N.A., Flynn, H., Adamson, J., et al. (2011). Expanded GGGGCC hexanucleotide repeat in noncoding region of *C9ORF72* causes chromosome 9p-linked FTD and ALS. Neuron *72*, 245–256.
4. Renton, A.E., Majounie, E., Waite, A., Simón-Sánchez, J., Rollinson, S., Gibbs, J.R., Schymick, J.C., Laaksovirta, H., van Swieten, J.C., Myllykangas, L., et al.; ITALSGEN Consortium (2011). A hexanucleotide repeat expansion in *C9ORF72* is the cause of chromosome 9p21-linked ALS-FTD. Neuron *72*, 257–268.
5. Ash, P.E.A., Bieniek, K.F., Gendron, T.F., Caulfield, T., Lin, W.-L., Dejesus-Hernandez, M., van Blitterswijk, M.M., Jansen-West, K., Paul, J.W., 3rd, Rademakers, R., et al. (2013). Unconventional translation of *C9ORF72* GGGGCC expansion generates insoluble polypeptides specific to c9FTD/ALS. Neuron *77*, 639–646.
6. Mori, K., Weng, S.-M., Arzberger, T., May, S., Rentzsch, K., Kremmer, E., Schmid, B., Kretzschmar, H.A., Cruts, M., Van Broeckhoven, C., et al. (2013). The *C9orf72* GGGGCC repeat is translated into aggregating dipeptide-repeat proteins in FTLD/ALS. Science *339*, 1335–1338.
7. Ciura, S., Lattante, S., Le Ber, I., Latouche, M., Tostivint, H., Brice, A., and Kabashi, E. (2013). Loss of function of *C9orf72* causes motor deficits in a zebrafish model of amyotrophic lateral sclerosis. Ann. Neurol. *74*, 180–187.
8. Therrien, M., Rouleau, G.A., Dion, P.A., and Parker, J.A. (2013). Deletion of C9ORF72 results in motor neuron degeneration and stress sensitivity in *C. elegans*. PLoS ONE *8*, e83450.
9. Prudencio, M., Belzil, V.V., Batra, R., Ross, C.A., Gendron, T.F., Pregent, L.J., Murray, M.E., Overstreet, K.K., Piazza-Johnston, A.E., Desaro, P., et al. (2015). Distinct brain transcriptome profiles in *C9orf72*-associated and sporadic ALS. Nat. Neurosci. *18*, 1175–1182.
10. Cooper-Knock, J., Bury, J.J., Heath, P.R., Wyles, M., Higginbottom, A., Gelsthorpe, C., Highley, J.R., Hautbergue, G., Rattray, M., Kirby, J., and Shaw, P.J. (2015). *C9ORF72* GGGGCC expanded repeats produce splicing dysregulation which correlates with disease severity in amyotrophic lateral sclerosis. PLoS ONE *10*, e0127376.
11. Cooper-Knock, J., Walsh, M.J., Higginbottom, A., Robin Highley, J., Dickman, M.J., Edbauer, D., Ince, P.G., Wharton, S.B., Wilson, S.A., Kirby, J., et al. (2014). Sequestration of multiple RNA recognition motif-containing proteins by *C9orf72* repeat expansions. Brain *137*, 2040–2051.
12. Lee, Y.B., Chen, H.J., Peres, J.N., Gomez-Deza, J., Attig, J., Stalekar, M., Troakes, C., Nishimura, A.L., Scotter, E.L., Vance, C., et al. (2013). Hexanucleotide repeats in ALS/FTD form length-dependent RNA foci, sequester RNA binding proteins, and are neurotoxic. Cell Rep. *5*, 1178–1186.
13. Waite, A.J., Bäumer, D., East, S., Neal, J., Morris, H.R., Ansorge, O., and Blake, D.J. (2014). Reduced C9orf72 protein levels in frontal cortex of amyotrophic lateral sclerosis and frontotemporal degeneration brain with the *C9ORF72* hexanucleotide repeat expansion. Neurobiol. Aging *35*, 1779.e5–1779.e13.
14. Levine, T.P., Daniels, R.D., Gatta, A.T., Wong, L.H., and Hayes, M.J. (2013). The product of C9orf72, a gene strongly implicated in neurodegeneration, is structurally related to DENN Rab-GEFs. Bioinformatics *29*, 499–503.
15. Zhang, D., Iyer, L.M., He, F., and Aravind, L. (2012). Discovery of novel DENN proteins: implications for the evolution of eukaryotic intracellular membrane structures and human disease. Front. Genet. *3*, 283.
16. Stenmark, H. (2009). Rab GTPases as coordinators of vesicle traffic. Nat. Rev. Mol. Cell Biol. *10*, 513–525.
17. Farg, M.A., Sundaramoorthy, V., Sultana, J.M., Yang, S., Atkinson, R.A.K., Levina, V., Halloran, M.A., Gleeson, P.A., Blair, I.P., Soo, K.Y., et al. (2014). C9ORF72, implicated in amytrophic lateral sclerosis and frontotemporal dementia, regulates endosomal trafficking. Hum. Mol. Genet. *23*, 3579–3595.
18. Amick, J., Roczniak-Ferguson, A., and Ferguson, S.M. (2016). C9orf72 binds SMCR8, localizes to lysosomes, and regulates mTORC1 signaling. Mol. Biol. Cell *27*, 3040–3051.
19. Sullivan, P.M., Zhou, X., Robins, A.M., Paushter, D.H., Kim, D., Smolka, M.B., and Hu, F. (2016). The ALS/FTLD associated protein C9orf72 associates with SMCR8 and WDR41 to regulate the autophagy-lysosome pathway. Acta Neuropathol. Commun. *4*, 51.
20. Webster, C.P., Smith, E.F., Bauer, C.S., Moller, A., Hautbergue, G.M., Ferraiuolo, L., Myszczynska, M.A., Higginbottom, A., Walsh, M.J., Whitworth, A.J., et al. (2016). The C9orf72 protein interacts with Rab1a and the ULK1 complex to regulate initiation of autophagy. EMBO J. *35*, 1656–1676.
21. Shi, Y., Lin, S., Staats, K.A., Li, Y., Chang, W.-H., Hung, S.-T., Hendricks, E., Linares, G.R., Wang, Y., Son, E.Y., et al. (2018). Haploinsufficiency leads to neurodegeneration in *C9ORF72* ALS/FTD human induced motor neurons. Nat. Med. *24*, 313–325.
22. Grant, B., and Hirsh, D. (1999). Receptor-mediated endocytosis in the *Caenorhabditis elegans* oocyte. Mol. Biol. Cell *10*, 4311–4326.
23. Kimble, J., and Sharrock, W.J. (1983). Tissue-specific synthesis of yolk proteins in *Caenorhabditis elegans*. Dev. Biol. *96*, 189–196.
24. Chotard, L., Skorobogata, O., Sylvain, M.-A., Shrivastava, S., and Rocheleau, C.E. (2010). TBC-2 is required for embryonic yolk protein storage and larval survival during L1 diapause in *Caenorhabditis elegans*. PLoS ONE *5*, e15662.
25. Xiao, S., MacNair, L., McGoldrick, P., McKeever, P.M., McLean, J.R., Zhang, M., Keith, J., Zinman, L., Rogaeva, E., and Robertson, J. (2015). Isoform-specific antibodies reveal distinct subcellular localizations of C9orf72 in amyotrophic lateral sclerosis. Ann. Neurol. *78*, 568–583.
26. Gallegos, M.E., Balakrishnan, S., Chandramouli, P., Arora, S., Azameera, A., Babushekar, A., Bargoma, E., Bokhari, A., Chava, S.K., Das, P., et al.

(2012). The *C. elegans* rab family: identification, classification and toolkit construction. PLoS ONE *7*, e49387.

27. Poteryaev, D., Datta, S., Ackema, K., Zerial, M., and Spang, A. (2010). Identification of the switch in early-to-late endosome transition. Cell *141*, 497–508.
28. Poteryaev, D., Fares, H., Bowerman, B., and Spang, A. (2007). *Caenorhabditis elegans* SAND-1 is essential for RAB-7 function in endosomal traffic. EMBO J. *26*, 301–312.
29. Chen, W., Feng, Y., Chen, D., and Wandinger-Ness, A. (1998). Rab11 is required for trans-golgi network-to-plasma membrane transport and a preferential target for GDP dissociation inhibitor. Mol. Biol. Cell *9*, 3241–3257.
30. Huber, L.A., Pimplikar, S., Parton, R.G., Virta, H., Zerial, M., and Simons, K. (1993). Rab8, a small GTPase involved in vesicular traffic between the TGN and the basolateral plasma membrane. J. Cell Biol. *123*, 35–45.
31. Kimura, K., and Kimura, A. (2012). Rab6 is required for the exocytosis of cortical granules and the recruitment of separase to the granules during the oocyte-to-embryo transition in *Caenorhabditis elegans*. J. Cell Sci. *125*, 5897–5905.
32. Chaineau, M., Ioannou, M.S., and McPherson, P.S. (2013). Rab35: GEFs, GAPs and effectors. Traffic *14*, 1109–1117.
33. Bucci, C., Parton, R.G., Mather, I.H., Stunnenberg, H., Simons, K., Hoflack, B., and Zerial, M. (1992). The small GTPase rab5 functions as a regulatory factor in the early endocytic pathway. Cell *70*, 715–728.
34. Hadano, S., Hand, C.K., Osuga, H., Yanagisawa, Y., Otomo, A., Devon, R.S., Miyamoto, N., Showguchi-Miyata, J., Okada, Y., Singaraja, R., et al. (2001). A gene encoding a putative GTPase regulator is mutated in familial amyotrophic lateral sclerosis 2. Nat. Genet. *29*, 166–173.
35. Yang, Y., Hentati, A., Deng, H.-X., Dabbagh, O., Sasaki, T., Hirano, M., Hung, W.-Y., Ouahchi, K., Yan, J., Azim, A.C., et al. (2001). The gene encoding alsin, a protein with three guanine-nucleotide exchange factor domains, is mutated in a form of recessive amyotrophic lateral sclerosis. Nat. Genet. *29*, 160–165.
36. Chun, D.K., McEwen, J.M., Burbea, M., and Kaplan, J.M. (2008). UNC-108/Rab2 regulates postendocytic trafficking in *Caenorhabditis elegans*. Mol. Biol. Cell *19*, 2682–2695.
37. Sellier, C., Campanari, M.-L., Julie Corbier, C., Gaucherot, A., Kolb-Cheynel, I., Oulad-Abdelghani, M., Ruffenach, F., Page, A., Ciura, S., Kabashi, E., and Charlet-Berguerand, N. (2016). Loss of C9ORF72 impairs autophagy and synergizes with polyQ Ataxin-2 to induce motor neuron dysfunction and cell death. EMBO J. *35*, 1276–1297.
38. Petit, C.S., Roczniak-Ferguson, A., and Ferguson, S.M. (2013). Recruitment of folliculin to lysosomes supports the amino acid-dependent activation of Rag GTPases. J. Cell Biol. *202*, 1107–1122.
39. Zhang, S., Ma, C., and Chalfie, M. (2004). Combinatorial marking of cells and organelles with reconstituted fluorescent proteins. Cell *119*, 137–144.
40. Jeong, D.-E., Lee, D., Hwang, S.-Y., Lee, Y., Lee, J.-E., Seo, M., Hwang, W., Seo, K., Hwang, A.B., Artan, M., et al. (2017). Mitochondrial chaperone HSP-60 regulates anti-bacterial immunity via p38 MAP kinase signaling. EMBO J. *36*, 1046–1065.
41. Hadwiger, G., Dour, S., Arur, S., Fox, P., and Nonet, M.L. (2010). A monoclonal antibody toolkit for *C. elegans*. PLoS ONE *5*, e10161.
42. Kostich, M., Fire, A., and Fambrough, D.M. (2000). Identification and molecular-genetic characterization of a LAMP/CD68-like protein from *Caenorhabditis elegans*. J. Cell Sci. *113*, 2595–2606.
43. Guo, P., Hu, T., Zhang, J., Jiang, S., and Wang, X. (2010). Sequential action of *Caenorhabditis elegans* Rab GTPases regulates phagolysosome formation during apoptotic cell degradation. Proc. Natl. Acad. Sci. USA *107*, 18016–18021.
44. Hermann, G.J., Schroeder, L.K., Hieb, C.A., Kershner, A.M., Rabbitts, B.M., Fonarev, P., Grant, B.D., and Priess, J.R. (2005). Genetic analysis of lysosomal trafficking in *Caenorhabditis elegans*. Mol. Biol. Cell *16*, 3273–3288.
45. Fares, H., and Greenwald, I. (2001). Regulation of endocytosis by CUP-5, the *Caenorhabditis elegans* mucolipin-1 homolog. Nat. Genet. *28*, 64–68.
46. Yu, L., McPhee, C.K., Zheng, L., Mardones, G.A., Rong, Y., Peng, J., Mi, N., Zhao, Y., Liu, Z., Wan, F., et al. (2010). Termination of autophagy and reformation of lysosomes regulated by mTOR. Nature *465*, 942–946.
47. Mrakovic, A., Kay, J.G., Furuya, W., Brumell, J.H., and Botelho, R.J. (2012). Rab7 and Arl8 GTPases are necessary for lysosome tubulation in macrophages. Traffic *13*, 1667–1679.
48. Li, Y., Chen, B., Zou, W., Wang, X., Wu, Y., Zhao, D., Sun, Y., Liu, Y., Chen, L., Miao, L., et al. (2016). The lysosomal membrane protein SCAV-3 maintains lysosome integrity and adult longevity. J. Cell Biol. *215*, 167–185.
49. Lu, N., Yu, X., He, X., and Zhou, Z. (2009). Detecting apoptotic cells and monitoring their clearance in the nematode *Caenorhabditis elegans*. Methods Mol. Biol. *559*, 357–370.
50. Tian, Y., Li, Z., Hu, W., Ren, H., Tian, E., Zhao, Y., Lu, Q., Huang, X., Yang, P., Li, X., et al. (2010). *C. elegans* screen identifies autophagy genes specific to multicellular organisms. Cell *141*, 1042–1055.
51. Kimura, S., Noda, T., and Yoshimori, T. (2007). Dissection of the autophagosome maturation process by a novel reporter protein, tandem fluorescent-tagged LC3. Autophagy *3*, 452–460.
52. Yang, M., Liang, C., Swaminathan, K., Herrlinger, S., Lai, F., Shiekhattar, R., and Chen, J.-F. (2016). A C9ORF72/SMCR8-containing complex regulates ULK1 and plays a dual role in autophagy. Sci. Adv. *2*, e1601167.
53. O'Rourke, J.G., Bogdanik, L., Yáñez, A., Lall, D., Wolf, A.J., Muhammad, A.K.M.G., Ho, R., Carmona, S., Vit, J.P., Zarrow, J., et al. (2016). *C9orf72* is required for proper macrophage and microglial function in mice. Science *351*, 1324–1329.
54. Cooper-Knock, J., Hewitt, C., Highley, J.R., Brockington, A., Milano, A., Man, S., Martindale, J., Hartley, J., Walsh, T., Gelsthorpe, C., et al. (2012). Clinico-pathological features in amyotrophic lateral sclerosis with expansions in C9ORF72. Brain *135*, 751–764.
55. Al-Sarraj, S., King, A., Troakes, C., Smith, B., Maekawa, S., Bodi, I., Rogelj, B., Al-Chalabi, A., Hortobágyi, T., and Shaw, C.E. (2011). p62 positive, TDP-43 negative, neuronal cytoplasmic and intranuclear inclusions in the cerebellum and hippocampus define the pathology of *C9orf72*-linked FTLD and MND/ALS. Acta Neuropathol. *122*, 691–702.
56. McCombe, P.A., and Henderson, R.D. (2011). The Role of immune and inflammatory mechanisms in ALS. Curr. Mol. Med. *11*, 246–254.
57. Van Den Bosch, L., Van Damme, P., Bogaert, E., and Robberecht, W. (2006). The role of excitotoxicity in the pathogenesis of amyotrophic lateral sclerosis. Biochim. Biophys. Acta *1762*, 1068–1082.
58. Westergard, T., Jensen, B.K., Wen, X., Cai, J., Kropf, E., Iacovitti, L., Pasinelli, P., and Trotti, D. (2016). Cell-to-cell transmission of dipeptide repeat proteins linked to *C9orf72*-ALS/FTD. Cell Rep. *17*, 645–652.
59. Clark, S.G., Lu, X., and Horvitz, H.R. (1994). The *Caenorhabditis elegans* locus *lin-15*, a negative regulator of a tyrosine kinase signaling pathway, encodes two different proteins. Genetics *137*, 987–997.
60. Chai, Y., Li, W., Feng, G., Yang, Y., Wang, X., and Ou, G. (2012). Live imaging of cellular dynamics during *Caenorhabditis elegans* postembryonic development. Nat. Protoc. *7*, 2090–2102.
61. Miesenböck, G., De Angelis, D.A., and Rothman, J.E. (1998). Visualizing secretion and synaptic transmission with pH-sensitive green fluorescent proteins. Nature *394*, 192–195.
62. Brenner, S. (1974). The genetics of *Caenorhabditis elegans*. Genetics *77*, 71–94.
63. Timmons, L., and Fire, A. (1998). Specific interference by ingested dsRNA. Nature *395*, 854.
64. Rual, J.F., Ceron, J., Koreth, J., Hao, T., Nicot, A.-S., Hirozane-Kishikawa, T., Vandenhaute, J., Orkin, S.H., Hill, D.E., van den Heuvel, S., and Vidal, M. (2004). Toward improving *Caenorhabditis elegans* phenome mapping with an ORFeome-based RNAi library. Genome Res. *14* (10B), 2162–2168.

65. Fraser, A.G., Kamath, R.S., Zipperlen, P., Martinez-Campos, M., Sohrmann, M., and Ahringer, J. (2000). Functional genomic analysis of *C. elegans* chromosome I by systematic RNA interference. Nature *408*, 325–330.

66. Fukushige, T., Hawkins, M.G., and McGhee, J.D. (1998). The GATA-factor *elt-2* is essential for formation of the *Caenorhabditis elegans* intestine. Dev. Biol. *198*, 286–302.

67. Mello, C.C., Kramer, J.M., Stinchcomb, D., and Ambros, V. (1991). Efficient gene transfer in *C.elegans*: extrachromosomal maintenance and integration of transforming sequences. EMBO J. *10*, 3959–3970.

68. Korčeková, D., Gombitová, A., Raška, I., Cmarko, D., and Lanctôt, C. (2012). Nucleologenesis in the *Caenorhabditis elegans* embryo. PLoS ONE *7*, e40290.

69. Davis, M.W., Hammarlund, M., Harrach, T., Hullett, P., Olsen, S., and Jorgensen, E.M. (2005). Rapid single nucleotide polymorphism mapping in *C. elegans*. BMC Genomics *6*, 118.

70. James, P., Halladay, J., and Craig, E.A. (1996). Genomic libraries and a host strain designed for highly efficient two-hybrid selection in yeast. Genetics *144*, 1425–1436.

71. Knop, M., Siegers, K., Pereira, G., Zachariae, W., Winsor, B., Nasmyth, K., and Schiebel, E. (1999). Epitope tagging of yeast genes using a PCR-based strategy: more tags and improved practical routines. Yeast *15* (10B), 963–972.

72. Wählby, C., Conery, A.L., Bray, M.-A., Kamentsky, L., Larkins-Ford, J., Sokolnicki, K.L., Veneskey, M., Michaels, K., Carpenter, A.E., and O'Rourke, E.J. (2014). High- and low-throughput scoring of fat mass and body fat distribution in *C. elegans*. Methods *68*, 492–499.

STAR★METHODS

KEY RESOURCES TABLE

REAGENT OR RESOURCE	SOURCE	IDENTIFIER
Antibodies		
Rabbit polyclonal anti-HA tag	Abcam	Cat#ab9110; RRID:AB_307019
Rabbit polyclonal anti-ALFA-1 #117	This paper	N/A
Mouse monoclonal anti-LMP-1	Nonet, [41]	Cat#LMP1; RRID:AB_2161795
Mouse Anti-beta-Tubulin Monoclonal Antibody	Sigma-Aldrich	Cat#T5293; RRID:AB_477580
Goat anti-rabbit secondary antibody (Alexa 488)	Thermo Fisher Scientific	Cat#A-11034; RRID:AB_2576217
Goat anti-mouse secondary antibody (Alexa 488)	Thermo Fisher Scientific	Cat#A-11001; RRID:AB_2534069
Peroxidase-conjugated Goat anti-mouse IgG secondary antibody	Thermo Fisher Scientific	Cat#G-21040; RRID:AB_2536527
Peroxidase-conjugated Goat anti-mouse IgG secondary antibody	Thermo Fisher Scientific	Cat#G-21234; RRID:AB_2536530
Bacterial and Virus Strains		
C. elegans, *E. coli* and *S. cerevisiae* strains	This paper	Table S2
Chemicals, Peptides, and Recombinant Proteins		
Recombinant protein: GST:ALFA-1(124-190)	This paper	N/A
Recombinant protein: MBP:ALFA-1(124-190)	This paper	N/A
Chemical: Isopropyl-β-D-thiogalactopyranoside	Amresco	Cat#0487
Chemical: Acetone	Sigma-Aldrich	Cat#650501
Chemical: Methanol	Sigma-Aldrich	Cat#34860
Chemical: Ethyl methanesulfonate	Sigma-Aldrich	Cat#M0880
Chemical: Western Lightning ECL Pro	PerkinElmer	Cat#NEL120E001EA
Chemical: cOmplete EDTA-free Protease Inhibitor cocktail	Sigma-Aldrich	Cat#11873580001
Chemical: glutathione Sepharose 4B	GE Healthcare	Cat#17075601
Chemical: Affi-Gel 10 Gel	Bio Rad	Cat#1536099
Chemical: Any kD Mini-PROTEAN TGX precast protein gel	Bio Rad	Cat#4569033
Chemical: 3-Amino-1,2,4-triazole (3-AT)	Sigma-Aldrich	Cat#A8056
Chemical: Oil Red O	Sigma-Aldrich	Cat#O0625
Critical Commercial Assays		
In-Fusion HD Cloning System	TaKaRa	Cat#639637
Zero Blunt TOPO PCR Cloning Kit	Thermo Fisher Scientific	Cat# K280020
Experimental Models: Organisms/Strains		
C. elegans, *E. coli* and *S. cerevisiae* strains	This paper	Table S2
Oligonucleotides		
Forward primer to amplify *Pvit-2::vit-2::5xGly*: ataggagaagtatatg aaacttcatctgaaaaacaac	This paper	AC663
Reverse primer to amplify *Pvit-2::vit-2::5xGly*: TCCTCCtccTCCT CCataagcgacgcaggcgg	This paper	AC664
Forward primer to amplify BFP (to generate *vit-2::bfp*): cagg cccggg GGAGGAGGAGGAGGAATGTCAGAGCTTATTAAGGAGAATATG CATAT	This paper	AC819
Reverse primer to amplify BFP (to generate *vit-2::bfp*): cagg GCGGCC gctaGCttaATTAAGCTTGTGACCCAGTTTGCTC	This paper	AC820
Forward primer to amplify *pHluorin* (to generate *vit-2::pHluorin*): cagg cccggg GGAGGAGGAGGAGGA atgagtaaaggagaagaactttttca	This paper	AC737
Reverse primer to amplify *pHluorin* (to generate *vit-2::pHluorin*): ACAGCGGCCgctaGCttaTTTGTATAGTTCATCCATG	This paper	AC982
Forward primer to amplify *alfa-1* promoter (until Exon 2) (to generate *Palfa-1::nls::gfp::unc-54 3′UTR*): cagg TCTAGA cgattccatcatgtcc aggatatcca	This paper	AC337

(*Continued on next page*)

Continued

REAGENT OR RESOURCE	SOURCE	IDENTIFIER
Reverse primer to amplify *alfa-1* promoter (until Exon 2)(to generate *Palfa-1::nls::gfp::unc-54 3′UTR*): cagg CCCGGG GTACAGCGTGAT CTTTCTTTTGTTG	This paper	AC338
Forward primer to amplify *alfa-1* UTR (to generate Palfa-1::nls::gfp:: alfa-1 3′UTR): cagg ACCGGT ttagccaaagtccaaaccagtcatgg	This paper	AC552
Reverse primer to amplify *alfa-1* UTR (to generate *Palfa-1::nls::gfp:: alfa-1* 3′UTR): cagg GGGCCC gttgatgctcttaactctgtcgaatttgac	This paper	AC553
Additional oligonucleotides	This paper	Table S1
Recombinant DNA		
Plasmid: pL15eK	[59]	N/A
Plasmid: BFP	Ou, [60]	N/A
Plasmid: pHluorin	[61]	N/A
Plasmid: *vit-2::BFP*	This paper	N/A
Plasmid: *vit-2::pHluorin*	This paper	N/A
Plasmid: vit-2::mCherry	This paper	N/A
Plasmid: *Palfa-1::alfa-1::HA*	This paper	N/A
Plasmid: *Palfa-1::ceC9orf72::HA*	This paper	N/A
Plasmid: *Pelt-2::alfa-1*	This paper	N/A
Plasmid: *sqst-1::mCherry::gfp*	This paper	N/A
Plasmid: pGBKT7	Clonetech	Cat#630443
Plasmid: pGAD	Clonetech	Cat#630442
Plasmid: pGBKT7-ALFA-1	This paper	N/A
Plasmid: pGBKT7-C9orf72	This paper	N/A
Plasmid: pGAD-SMCR-8	This paper	N/A
Plasmid: pGAD-FLCN-1	This paper	N/A
Plasmid: pIJ658	Lee, [40]	N/A
Plasmid: pIJ659	Lee, [40]	N/A
Plasmid: *alfa-1::spGFPN*	This paper	N/A
Plasmid: *ceC9orf72::spGFPN*	This paper	N/A
Plasmid: *smcr-8::spGFPC*	This paper	N/A
Plasmid: *flcn-1::spGFPC*	This paper	N/A
Plasmid: pGEX-4T-1 GST-ALFA-1(124-190)	This paper	N/A
Plasmid: pMALc2 MBP-ALFA-1(124-190)	This paper	N/A
Plasmid: pL4440-*K02E10.1*	This paper	N/A
Plasmid: pL4440-*Y71H2AM.12*	This paper	N/A
PCR product: *smcr-8* rescue	This paper	N/A
Software and Algorithms		
ImageJ	NIH	https://imagej.nih.gov/ij/
GraphPad Prism 6 and 7	GraphPad Software	https://www.graphpad.com/scientific-software/prism/
Zen Blue and Lite Editions	Zeiss	https://www.zeiss.com/microscopy/us/downloads/zen.html

CONTACT FOR REAGENT AND RESOURCE SHARING

Further information and requests for resources and reagents should be directed to and will be fulfilled by the Lead Contact, H. Robert Horvitz (horvitz@mit.edu).

EXPERIMENTAL MODEL AND SUBJECT DETAILS

C. elegans hermaphrodite strains were maintained on Nematode Growth Medium (NGM) plates containing 3 g/L NaCl, 2.5 g/L peptone and 17 g/L agar supplemented with 1 mM $CaCl_2$, 1 mM $MgSO_4$, 1 mM KPO_4 and 5 mg/L Cholesterol with *E. coli* OP50

as a source of food [62]. All strains were derived from the Bristol N2 wild-type strain and are listed in Table S2. All strains were maintained at 20°C. RNAi treatments were performed by feeding animals with HT115 bacteria containing different RNAi constructs [63–65]. Unless otherwise stated, 25-30 L1 larvae were placed onto each NGM plate containing 1 mM isopropyl-β-D-thiogalactoside and 100 μg/mL and about 72 hr later the progeny of these animals were scored for presence of blobs. Control RNAi treatments were performed using the empty vector pL4440. The names of the RNAi clones used in this study are provided in the Table S2.

METHOD DETAILS

Plasmids

The $P_{alfa\text{-}1}$*::4xnls::gfp* transcriptional reporter was constructed using PCR to amplify a 2.5cKb fragment upstream of *alfa-1* into 25 nucleotides in exon 2, to include the two alternative first exons in *alfa-1*. The resulting amplicon was digested with XbaI and SmaI and ligated into pPD122.56, which encodes a 4xNLS::GFP fusion to generate $P_{alfa\text{-}1}$*::4xnls::gfp::unc-54 3′UTR*. *unc-54 3′UTR* was replaced by the 1.0 Kb region downstream of the stop codon of *alfa-1*. The $P_{alfa\text{-}1}$*::alfa-1 gDNA::3xGly::HA::alfa-1 3′ UTR* was generated using site-directed mutagenesis of the plasmid $P_{alfa\text{-}1}$*::alfa-1 gDNA::alfa-1 3′ UTR*, which contains 2.5 Kb 5′ of *alfa-1*, the full-length *alfa-1* gDNA and 1.0 Kb 3′ of the stop codon of *alfa-1*. $P_{alfa\text{-}1}$*::ceC9orf72 cDNA::3xGly::HA::alfa-1 3′ UTR* was generated from $P_{alfa\text{-}1}$*::alfa-1 gDNA::3xGly::HA::alfa-1 3′ UTR* by blunt ligation of a wild-type human *C9orf72* cDNA codon-optimized for expression in *C. elegans* containing three synthetic introns generated using gBlocks Gene Fragments (Integrated DNA Technologies) after the eighth amino acid of *alfa-1* exon 2 and eliminating the downstream *alfa-1* ORF. The *ceC9orf72* sequence is shown as supplementary information. The *vit-2* reporters were cloned in the pRS426 plasmid and contain 1 Kb of the promoter and the full-length *vit-2* gDNA, followed by a linker of five glycines and the specified fluorescent protein (mCherry, BFP or pHluorin) and the *unc-54* 3′UTR. For the split-GFP protein-protein *in vivo* interaction assay, all cloning was performed using the Clontech In-Fusion system. The C-terminal GFP (spGFPC) fragment was cloned between *alfa-1* or *C9orf72* and the *alfa-1* 3′UTR. To generate the empty spGFPC transgene, spGFPC was cloned between the *alfa-1* promoter and the 3′UTR. The *smcr-8::spGFPN* transgene was generated by first cloning an *smcr-8* PCR product encompassing a region from 1.2 Kb upstream to 250 bp downstream of *smcr-8* ORF using a Zero Blunt TOPO PCR Cloning Kit and then adding the spGFPN fragment between smcr-8 ORF and 3′UTR. Once this plasmid was generated, to construct the *flcn-1::spGFPN* transgene we substituted the *smcr-8* ORF with a *flcn-1a* cDNA. The *sqst-1::mCherry::gfp* reporter was cloned in the pRS426 plasmid and contained 2.5 Kb of the promoter and the full-length *sqst-1* gDNA [50], followed by mCherry and GFP fluorescent genes, with a linker of three glycines between each ORF, followed by the *unc-54* 3′UTR. The $P_{elt\text{-}2}$*::alfa-1::unc-54 3′UTR* transgene was cloned by replacing the *alfa-1* promoter in a $P_{alfa\text{-}1}$*::alfa-1 gDNA::unc-54 3′ UTR* transgene derived from $P_{alfa\text{-}1}$*::4xnls::gfp* with the promoter of the *elt-2* gene [66]. The specific primer sequences are described in Key Resources Table and Table S1.

Germline transformation

Germline transformation was performed by injecting the specified amounts of the indicated plasmids into the gonads of one-day adults. F1 animals containing the extrachromosomal array were singled into individual plates and those transmitting the array to their progeny were maintained to generate independent transgenic lines [67]. *alfa-1* and *ceC9orf72* translational reporters were injected at 50 μg/mL into *alfa-1(ok3062); lin-15(n765)* animals with 20 μg/mL of the indicated fluorescent markers and 40 μg/mL of the *lin-15(n765)*-rescuing plasmid pL15EK as co-injection markers [59]. A *smcr-8* PCR product encompassing 1.2 Kb upstream to 250 bp downstream of *smcr-8* ORF was injected in *smcr-8(n5788)* and *smcr-8(gk173828)* animals at 50 μg/mL with 20 μg/mL of the ubiquitously expressed $P_{sur\text{-}5}$*::nls::gfp* marker. Vitellogenin fluorescent reporters were injected at 50 μg/mL into *lin-15(n765)* or *alfa-1(ok3062); lin-15(n765)* animals with 40cμg/mL of pL15EK as a co-injection marker. The *nIs755* transgene was generated by injection of 50 μg/mL of *vit-2::BFP* and 50 μg/mL of *vit-2::pHluorin* transgenes into *alfa-1(ok3062); wjIs51* animals. Extrachrosomal arrays were integrated by gamma-ray irradiation (4,800 rads) of transgene-carrying L4 animals. For the split-GFP protein-protein *in vivo* interaction assay, wild-type animals were injected with 50 μg/mL of the spGFPN-containing transgene, 50 μg/mL of the spGFPC-containing transgene and 5 μg/mL *Pges-1::mCherry*, used as co-injection marker.

Starvation survival assay

Synchronized L1 larvae were incubated in 2.5 mL of sterilized M9 buffer on a rocker at 20°C for the times indicated. Approximately 100 worms were placed on individual seeded plates at the indicated times. The number of survivors was determined after 3 days at 20°C. Day 1 is considered to be the first day of starvation and was used as the 100% survival point.

Microscopy, immunohistochemistry and image analysis

Nomarski DIC and epifluorescence micrographs were obtained using an Axioskop II (Zeiss) compound microscope and OpenLab software (Agilent). Confocal microscopy was performed using Zeiss LSM 510, LSM 710 and LSM 800 instruments. The resulting images were prepared using ImageJ software (National Institutes of Health). Image acquisition settings were calibrated to minimize the number of saturated pixels and were kept constant throughout each experiment. Graphs and indicated statistical analyses were performed using Microsoft Excel and GraphPad Prism 6 and 7 softwares. For immunohistochemistry, fixing the samples were fixed for 5 min at −20°C in methanol followed by incubation at −20°C in acetone. Samples were then rehydrated through 70%, 50% and 30% ice-cold acetone in PBS [68]. anti-HA primary antibody (ab9110, Abcam) incubation was overnight at 4°C. Secondary antibody was

goat anti-rabbit antibody coupled with Alexa 488 (1:2500) (Invitrogen). Images were acquired using a Zeiss LSM 510 confocal microscope. To determine lysosomal tubulation and reformation (Figure 4H), we took Z stack images using Zeiss LSM 800 confocal microscope at 0.37 μm z-intervals every ≈14 s. To quantify lysosomal tubule length (Figure 4I), we photographed the hypoderm of comma-stage embryos carrying the *nuc-1::mCherry* reporter, and the lengths of tubular structures were quantified using ImageJ. To determine the average time for phagolysosome formation or cell-corpse degradation (Figures 5E and 5F), we took Z stack images using Zeiss LSM 800 confocal microscope at 0.5 μm z-intervals every 2 min. To analyze the % of autophagosomes from the total of autophagosomes and autophagolysosomes (Figures 5G and 5H), we acquired images of the hypoderm of 2-fold embryos using a Zeiss LSM 800 confocal microscope and determined the number of particles positive for both GFP and mCherry (autophagosomes) and the number of particles positive for only mCherry (autophagolysosomes) uisng ImageJ. To detect the release and merging of blobs (Figure S1C), we took Z stack images using Zeiss LSM 710 or LSM 800 confocal microscopes at 0.3-0.5 μm z-intervals approximately every 70 s. To rule out the possibility of previously released blobs appearing from a focal plane not imaged, we excluded blobs initially visible in the first or last focal planes to ensure that we could detect their release. To detect the fusion of blobs (Figure S1E), we took Z stack images using Zeiss LSM 700 confocal microscope at 0.37 μm z-intervals approximately every 70 s.

Counts of blobs and persistent corpses

The penetrance of the blob phenotype, i.e., the percent of animals in which one or more blobs were visible, was quantified in embryos at the 3-fold stage or older but before initiation of pumping, derived from one-day adults unless otherwise stated. We used a × 100 objective equipped with Nomarski differential interference contrast (DIC) optics. The number of persistent cell corpses was scored by counting raised highly refractile dead cells in the head region of 1.5-fold stage embryos [49].

Genetic screen and mapping of smcr-8(n5788)

smcr-8(n5788) was isolated from a genetic screen of *rab-2(nu415); pwIs23 [vit-2::gfp]* animals for mutations that cause the F3 embryos that accumulate in the uteri of F2 progeny to contain large GFP-positive blobs. Mutagenesis was performed by treating synchronized L4 larvae with 0.05 M ethyl methanesulfonate (EMS) at 20°C for 4 hr. *smcr-8(n5788)* was identified by crossing the mutant isolate with a Hawaiian strain containing the *nIs755* reporter, isolating the F2 progeny with accumulated eggs with large blobs and mapping the mutation using single nucleotide polymorphisms [69] and whole-genome sequencing.

Antibody production and western blot analysis

A protein fragment corresponding to amino acids 124-190 of ALFA-1 fused to glutathione S- transferase (GST) was expressed, purified using glutathione Sepharose 4B (Amersham Biosciences) and used to raise rabbit anti-ALFA-1 antibodies. Antisera were generated by Pocono Rabbit Farm and Laboratory. Specific antibodies were affinity-purified using an identical ALFA-1 protein fragment fused to maltose-binding protein (MBP) and coupled to Affigel 10 (Bio-Rad). Protein extracts were prepared from *C. elegans* embryos of the indicated genotypes containing the yolk reporter *pwIs98[vit-2::tdimer2]*. 10 μg of total protein were loaded onto Any kD Mini-PROTEAN TGX precast protein gels and then transferred to nitrocellulose membranes. The membranes were probed with anti-ALFA-1 and mouse anti-tubulin (Sigma) antibodies. Immunocomplexes were detected using HRP-conjugated anti-rabbit or anti-mouse IgG secondary antibodies (Invitrogen) followed by chemiluminescence (Western Lightning ECL, PerkinElmer).

Yeast two-hybrid binding assay

alfa-1, *C9orf72*, *smcr-8* and *flcn-1a* cDNAs were cloned into pGBKT7 and pGADT7 plasmids, and the constructs were sequentially introduced into yeast strain PJ649A [70]. 1mL of exponentially growing yeasts were pelleted and resuspended in 70 μL of water. 10 μL of 10 μg/mL denatured salmon sperm, 1 μg of the desired DNA, 240 μL 50% PEG 3350 and 36 μL 1 M LiOAc were added to the resuspended yeasts. After 30' at room temperature, the mix was heat shocked for 15' at 42°C. Yeasts were washed with water and plated on the appropriate SD plates [71]. Single colonies were streaked and cultured for two days at 30°C on SD plates containing minimal supplements without tryptophan and leucine. To test yeast growth, yeast strains were grown overnight in liquid, and cultures were diluted to a similar optical density at 600 nm. Serial 4x dilutions were made in water, and 5 μL of each dilution was used to yield one spot. Plates were cultured for two days at 30°C on SD plates containing minimal supplements without tryptophan, leucine and histidine and containing 3 mM of the competitive inhibitor of histidine synthesis 3-AT.

Oil Red O (ORO) staining and imaging

Well-fed or food-deprived one-day adult worms were fixed by washing them in 60% isopropanol, stained overnight with 0.3% ORO in 60% isopropanol and washed with 1xPBS with 0.01% Triton [72]. Worms were imaged using a Nikon DS-Ri2 color camera coupled to a Nikon SMZ18 microscope.

ceC9orf72 sequence

The long isoform of C9orf72 was codon-optimized for expression in *C. elegans* and synthesized using gBlocks Gene Fragments (Integrated DNA Technologies). Three synthetic introns (in italics and lower case) were introduced to improve *ceC9orf72* expression.

ATGTCAACCCTCTGTCCACCACCGAGTCCAGCAGTTGCGAAAACTGAGATTGCTCTCTCTGGAAAATCCCCTCTCCTGGCCGCT
ACTTTCGCGTACTGGGATAATATTCTGGGACCACGAGTGCGTCATATTTGGGCCCCGAAAACAGAACAGGTACTCCTTAGCGATG
GTGAAATCACGTTCCTGGCAAATCACACGTTGAACGGAGAAATCCTTAGAAACGCGGAGTCAGGAGCCATTGATGTAAAATTTTTC
GTTCTCTCGGAGAAG*gtaagtttaaacatatatatactaactaaccctgattatttaaattttcag*GGTGTTATTATCGTTAGCCTGATTTTTGACGGTAACTG
GAACGGTGATCGTAGTACTTATGGCCTTAGTATTATTCTGCCACAAACTGAACTCTCTTTCTATCTTCCACTCCATCGAGTTTGCGT
AGATCGATTGACACATATAATAAGAAAAGGAAGAATTTGGATGCATAAAGAGCGTCAGGAGAATGTTCAAAAGATTATTCTTGAAGG
AACTGAACGAATGGAAGACCAAGGACAATCAATTATCCCAATGCTGACAGGCGAGGTGATTCCAGTTATGGAACTCTTATCATCGA
TGAAGTCGCACTCCGTTCCAGAGGAAATTGATATCGCCGATACGGTATTAAACGACGATGATATTGGCGATTCTTGCCACGAGGG
ATTCCTTCTTAATGCAATCTCCTCACACTTGCAAACTTGTGGTTGTTCAGTGGTTGTCGGATCTTCTGCCGAAAAG*gtaagtttaaacagtt*
*cggtactaactaaccatacatatttaaattttcag*GTGAATAAAATTGTCCGAACTCTGTGTCTCTTCTTGACCCCAGCAGAACGTAAATGTTCTCGA
CTGTGTGAGGCCGAGTCTTCTTTCAAATATGAAAGTGGATTGTTCGTGCAAGGACTTTTGAAAGATTCAACTGGATCTTTTGTCCTC
CCATTCCGACAAGTGATGTATGCCCCATACCCTACTACACACATCGATGTTGATGTAAATACGGTGAAGCAAATGCCACCGTGCCA
TGAGCACATCTATAATCAGCGACGTTACATGAGAAGCGAGCTTACAGCATTCTGGCGAGCTACATCCGAAGAAGATATGGCCCAA
GACACTATTATTTACACCGACGAGAGCTTTACGCCTGACCTGAACATATTTCAGGATGTTCTTCATCGAGACACCCTGGTCAAAGC
TTTTCTTGATCAAGTTTTCCAATTAAAACCAGGTCTGTCCCTCAGATCCACATTCTTAGCCCAATTTCTGCTTGTCTTACATCGTAAA
GCTCTGACTTTGATTAAGTACATTGAG*gtaagtttaaacatgattttactaactaactaatctgatttaaattttcag*GATGATACGCAAAAGGGAAAAAAAC
CTTTCAAATCACTTAGAAATCTCAAAATTGACCTCGATCTGACTGCAGAAGGAGATTTAAACATAATTATGGCCTTAGCAGAAAAGAT
CAAGCCAGGTTTACACTCTTTCATATTCGGAAGACCGTTTTATACAAGTGTTCAGGAGAGAGACGTGTTAATGACTTTT

QUANTIFICATION AND STATISTICAL ANALYSIS

Unless otherwise stated, for quantification of the blob phenotype penetrance, 100 embryos at the 3-fold stage or older but before initiation of pumping derived from one-day adults were scored per genotype or RNAi treatment. The average value and the standard deviation of the mean (s.e.m) of three independent experiments are shown. Non-parametric Student's t tests were used to determine statistical significance. For Figure 2A, multiple comparison one-way ANOVA was used to determine statistical significance. Graphs and indicated statistical analyses were performed using Microsoft Excel and GraphPad Prism 6 and 7 softwares. For colocalization coefficient quantification and VIT-2::BFP mean intensity quantification (Figures 4C and 4D), a region of interest (ROI) was drawn around each embryo, avoiding blobs and cell corpses. Another ROI was drawn inside the embryo where no reporter was visible to set the background threshold for each image. Analysis was performed with Zen software (Zeiss).